

Soft Matter

Morphology of Poly-3-hexyl-thiophene Blends with Styrene-Isoprene-Styrene Block-Copolymer Elastomers from X-Ray and Neutron Scattering

Journal:	Soft Matter
Manuscript ID	SM-ART-04-2024-000495.R1
Article Type:	Paper
Date Submitted by the Author:	01-Jul-2024
Complete List of Authors:	Scheiwiller, Sage; University of Washington, Chemical Engineering Mata, Jitendra; ANSTO; University of New South Wales Pozzo, Lilo; University of Washington

SCHOLARONE™ Manuscripts Page 1 of 51 Soft Matter

Morphology of Poly-3-hexyl-thiophene Blends with Styrene-Isoprene-Styrene Block-

Copolymer Elastomers from X-Ray and Neutron Scattering

Sage C. Scheiwiller [1], Jitendra Mata [2][3], and Lilo D. Pozzo* [1]

*Email: dpozzo@uw.edu

Affiliations

[1] Department of Chemical Engineering, University of Washington, Seattle, WA, USA

[2] Australian Centre for Neutron Scattering (ACNS), Australian Nuclear Science and Technology

Organisation (ANSTO), Lucas Heights, NSW 2234, Australia

[3] School of Chemistry, University of New South Wales, Sydney, NSW 2052, Australia

Abstract

The nano- and micron scale morphology of poly(3-hexylthiophene) (P3HT) and polystyrene-block-polyisoprene-block-polystyrene (PS-PI-PS) elastomeric blends is investigated through the use of ultra-small and small angle X-ray and neutron scattering (USAXS, SAXS, SANS). It is demonstrated that loading P3HT into elastomer matrices is possible with little distortion of the elastomeric structure up to a loading of ~5 wt%. Increased loadings of conjugated polymer is found to significantly distort the matrix structure. Changes in processing conditions are also found to affect the blend morphology with especially strong dependence on processing temperature. Processing temperatures above the glass transition temperature (T_g) of polystyrene and the melting temperature (T_m) of the conjugated polymer additive (P3HT) creates significantly more organized mesophase domains. P3HT blends with PS-PI-PS can also be flow-aligned through processing, which results in an anisotropic structure that could be useful for the generation of Soft Matter Page 2 of 51

anisotropic properties (e.g. conductivity). Moreover, the extent of flow alignment is significantly affected by the P3HT loading in the PS-PI-PS matrix. The work adds insight to the morphological understanding of a complex P3HT and PS-PI-PS polymer blend as conjugated polymer is added to the system. We also provide studies isolating the effect of processing changes aiding in the understanding of the structural changes in this elastomeric conjugated polymer blend.

Keywords

Keywords: Small Angle X-ray Scattering, conjugated polymers, elastomers, organic electronics

Page 3 of 51 Soft Matter

1- Introduction

1a- Elastomers

Elastomers are increasingly important materials for developments in the field of flexible electronics, including healthcare sensors^{1–3}, electronic skin^{4–6}, stretchable OLED⁷ displays^{8,9}, and flexible solar cells^{10–12}. These electronic technologies come in many forms, some with metallic circuits suspended on elastomeric substrates^{13,14}, others with resilient electronic fibers embedded within stretchable material^{15,16}, or even stretchable electronic material forming electrodes that can flex and move with a flexible device^{17,18}. The base of all these materials are elastomers in a variety of forms. An important family of thermoplastic elastomers are created from block copolymers, which consist of two or more sections of homopolymers that are bonded together. Typically, blocks of glassy polymers are used to create physical bonds that can be reversibly created and destroyed via changes in temperature. Such glassy-polymer blocks join with elastomeric blocks to provide the desired elastomeric properties while retaining the temperature processing that is not usually possible in typical thermoset elastomers (e.g. vulcanized rubbers).

Block copolymers (BCPs) can also be designed as diblock, triblock, or multiblock to create complex nanoscale architectures through self-assembly. In this work, we focus on a commonly used commercial triblock thermoplastic elastomer composed of styrene-based ABA copolymer polystyrene-block-polyisoprene-block-polystyrene (PS-PI-PS) (Figure 1a). Elastic properties emerge from the restoring force of this polymer, which are a result of physical crosslinks from glassy polystyrene (PS) end-blocks and the elastomeric nature of the polyisoprene (PI). These crosslinks involve non-covalent molecular associations that provide strength and structure while facilitating processing due to the possibility of thermally reversing the crosslinking process when heating above the glass transition temperature of polystyrene. Physical crosslinking in a PS-PI-PS

Soft Matter Page 4 of 51

polymer occurs when the hard glassy polystyrene blocks associate during processing and act as physical connections while the rubbery flexible polyisoprene block is able to deform and stretch¹⁹. These unique physical properties are a result of large difference in glass transition temperature between polystyrene ($T_g \sim 100~^{0}$ C) and polyisoprene ($T_g \sim -57~^{0}$ C)^{20,21}. The combination of flexible rubbery regions and glassy regions allows for the polymer to be mechanically strong, flexible, and resilient, as shown in **Figure 1c.**

Polystyrene and polyisoprene chains are also known to self-segregate into nanoscale phaseseparated morphologies including spherical micelles²², hexagonal cylinders^{23,24}, lamellar^{25,26}, gyrodal^{27,28}, and cubic crystals²⁹, depending on the polymer architecture ^{25,30}, temperature ³¹, and processing conditions ^{32,33}. The degree of polymerization of each block changes the ratio between them, and as established by calculations done by Matsen and Bates, the ratio between the A and B blocks facilitates specific structures to emerge.³⁰ In general, when styrene content is low, the PS-PI-PS copolymer forms polystyrene nano-spheres or micelles engulfed in an isoprene matrix. As the styrene fraction increases, the PS-PI-PS material transitions to form polystyrene cylinders dispersed in an isoprene matrix, then at near equal ratios alternating lamellar structures, and finally at high styrene loadings, creating polyisoprene microdomains within the bulk polystyrene. While the polymer structure has a strong influence on the specific phase that is formed, processing variables also affect the final structure by creating kinetically arrested states and/or altering their macroscopic orientation. For styrene percentages between 20-40%, solvent choice was found to be exceptionally important in determining phase structure, with samples tending to create continuous polystyrene microdomains when the solvent is more compatible with polystyrene than with polyisoprene^{22,34}. Qiao et al found that changing the solvent while casting PS-PI-PS or its inverse copolymer (i.e. polyisoprene-b-polystyrene-b-polyisoprene) at fixed molecular weights

Page 5 of 51 Soft Matter

and compositions, the phase structure could be changed from lamellar, cylindrical or gyroidal³². Sakurai et.al. also studied the effect of annealing on polystyrene-polybutadiene-polystyrene (SBS) elastomer, a closely related thermoplastic elastomer, and found that cast films that formed hexagonal cylinders would gradually transition into lamellae upon annealing above the glass transition of polystyrene³¹.

1b- Conjugated Polymer Additives

Further complexity in phase and structure emerges with the inclusion of additives into blends with thermoplastic elastomers like PS-PI-PS. For elastomeric electronics, additives have included carbon nanotubes^{35,36}, conjugated polymer nanowires^{15,37}, and 'dissolved' conjugated polymer chains in an elastomeric blend^{18,38,39}.

Conjugated polymers (CPs) are a unique subset of polymers with alternating saturated and unsaturated bonds along their backbones that allow for electron resonance through the chain, as well as across adjacent chains when found in sufficiently close configurations⁴⁰. Incorporating conjugated polymers into elastomers has been shown to open a field of new possibilities, by embedding elastomeric polymers with desired electronic properties^{39,41–44}. Elastic electronic materials are often subjected to long lifespans of continuous deformation, and often need to be thin and compact, requiring both mechanical durability and electronic efficiency. The addition of a conjugated polymeric additive allows for the unique combination of the elastomeric matrix's physical properties and the conjugated polymers optical and electronic properties even at low loadings (**Figure 1c-e**)^{42–44}. Experiments by Carpi et. al. with blends of polydimethylsiloxane and P3HT (**Figure 1b**) found that even small amounts of added conjugated polymer (1-6 wt%) showed increases in conductive properties, with a maximum in electromechanical response seen at 1wt% conjugated polymer³⁹. Simple blended materials often consist of two homopolymers and more

Soft Matter Page 6 of 51

complex systems, such as the replacement of the elastomeric homopolymer with a triblock copolymer, require further insight.

With the addition of a conjugated polymer into a triblock copolymer matrix, phase behavior increases in complexity as new interactions between the copolymer blocks and the conjugated polymers emerge. Intermolecular interactions between components ultimately drive these materials to reach a stable thermodynamic equilibrium. However, time scales for achieving equilibrium can be much longer than practical and solvent evaporation or processing frequently leads to kinetically arrested states. During solvent evaporation, the composition and physical properties of samples changes rapidly and unevenly, resulting in phase separation, and solventdependent formation of complex structures^{32,45,46}. In simulations, Cummings et al describes the phase segregation of drying solutions through multiple thermodynamic drivers and described how the evaporation of all solvent can lock in kinetically frozen structures⁴⁶. Depending on the kinetics of processing versus the thermodynamic drive, equilibrium may not be achieved for all practical purposes, resulting in materials with a processing dependent structure. Once dry, temporal fluctuations in amorphous materials are still observed, but often have slow time scales that can only be sped up through thermal or solvent annealing^{47–49}. Hadziioannou et al found that a PS-PI diblock copolymer formed lamellae of ~600 Å wide periods at room temperatures, and these expanded to 710 Å after annealing for 1000 hours at 182 °C. When exposed to higher temperatures (255 °C) the lamellar spacing reached values over 1000 Å within just 10 hours⁴⁹. In solid films, the balance between the kinetics of gradual chain movements and thermodynamics of the material cannot ensure that equilibrium is reached. This competition between kinetics and thermodynamics frequently determines the structural outcome with respect to processing techniques, component architecture, and applied conditions. Understanding changes to the structure of polymer blends Page 7 of 51 Soft Matter

throughout processing stages provides valuable insights into how specific steps and integration of conjugated polymer components affect the performance of composite electronic materials.

In this work we use small angle scattering of X-rays and neutrons and ultra small angle Xray scattering (SAXS, SANS, and USAXS) to analyze the molecular structure of complex polymer blends containing thermoplastic elastomers and conjugated polymers (P3HT). We hypothesize, based on previous work, that the conjugated polymer will preferentially integrate within the selfassembled polyisoprene domains until a critical loading concentration is reached and large-scale aggregation occurs. This is expected to result in phase-separation of the conjugated polymer outside of the structured elastomeric template^{50–53}. We further expect processing conditions, especially temperature history, to induce large structural changes and modification of the extent of organization^{49,54}. Changes induced by processing conditions can affect material use cases and we anticipate that, through intentional modification, widespread order and structural control can be manipulated⁵⁵. The influence of both composition and processing conditions on structural outcomes over multiple length scales is possible through the use of non-destructive sampling via solution-phase small angle neutron scattering (SANS), small angle x-ray scattering (SAXS), and ultra-small angle x-ray scattering (USAXS), as a function of processing variables and stages. This presents a detailed view of the relative impact of different processing steps on the structure of these important classes of composite materials.

Soft Matter Page 8 of 51

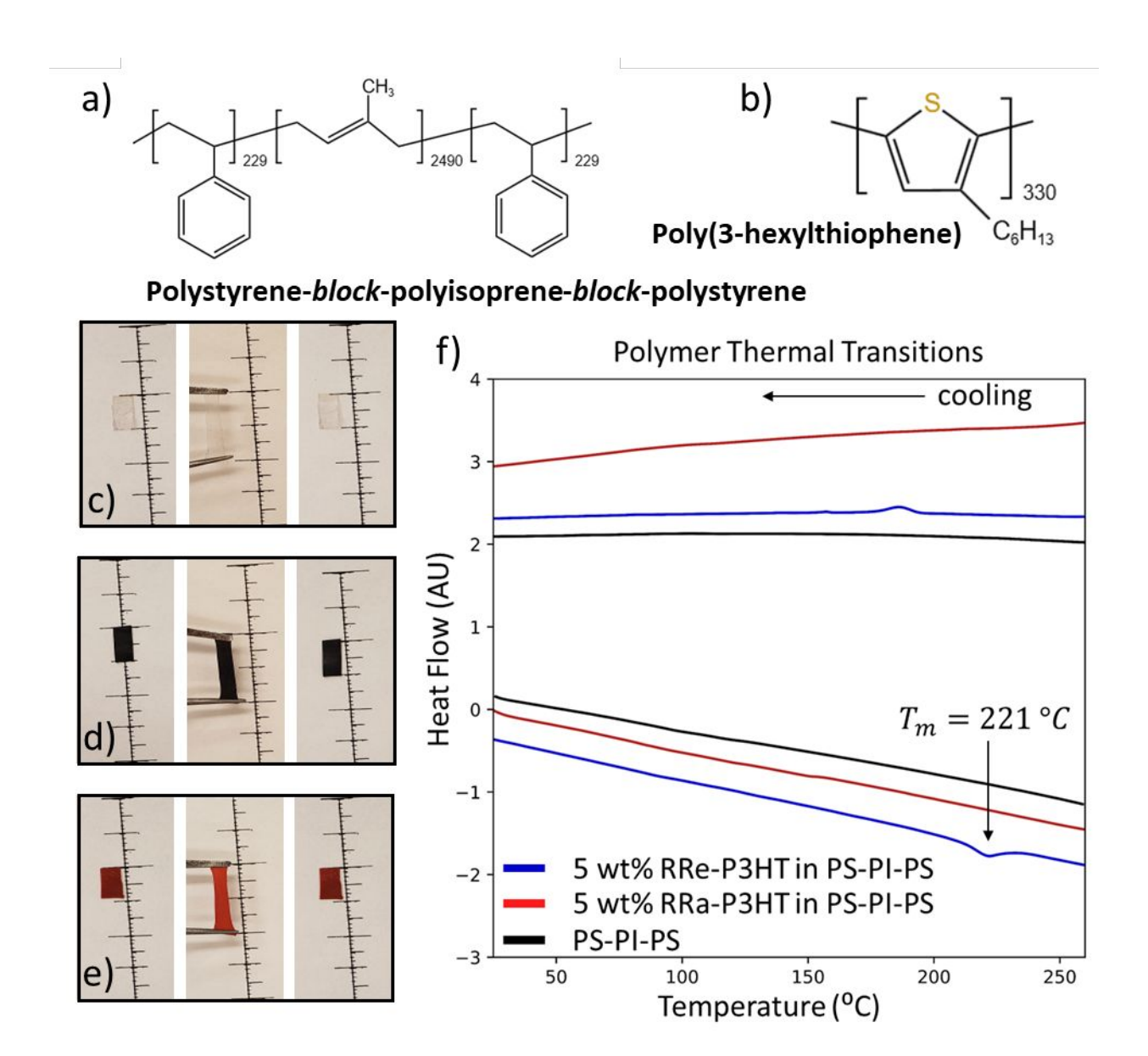


Figure 1. Polymer structures of a) polystyrene-block-polyisoprene-block-polystyrene (PS-PI-PS) elastomer block copolymer and b) poly(3-hexylthiophene) (P3HT) conjugated polymer. Images of representative templates and blends at rest before strain, under strain, and under rest after strain for c) PS-PI-PS d) 5 weight percent Regio-regular P3HT in PS-PI-PS blend e) 5 weight percent Regio-random P3HT in PS-PI-PS blend. f) Differential Scanning Calorimetry data collected for the representative templates and blends.

Page 9 of 51 Soft Matter

2- Materials and Methods

2a- Materials

Regio-random poly(3-hexylthiophene) (RRa-P3HT) (MW = 63 kg mol-1, D = 2.4, Product 4007) and Regio-regular poly(3-hexylthiophene) (RRe-P3HT) were purchased from Rieke Metals (Lincoln, NE USA). Three different molecular weights of RRe-P3HT were used: Lot BLS26-16 (RRe42) (MW = 42 kg mol-1, D = 2.0, RR = 90), Lot PTL43-54 (RRe60) (MW = 60 kg mol-1, D = 3.0, RR = 91) and Lot BLS26-96 (RRe77) (MW = 77 kg mol-1, D = 2.4, RR = 94). GPC (**Figure S2**) and NMR (**Figure S3**) are provided from Rieke Metals for all conjugated polymers. Polystyrene-block-Polystoprene-block-Polystyrene (PS-PI-PS) was purchased from Aldrich Chemistry (St. Louis, MO USA). The PS-PI-PS polymer is a 22% styrene $A_{229}B_{2490}A_{229}$ triblock-copolymer with a molecular weight of 217,000 Da as determined using Gel Permeation Chromatography (GPC), shown in **Figure S1**. Chloroform was purchased from Fisher Chemical (Waltham, MA USA). For SANS experiments, fully deuterated chloroform was purchased from Cambridge Isotope Laboratories, Inc. (Tewksbury, MA USA). All chemicals were used as received.

2b- Heat-Pressed Film Preparation

All solid blend films were prepared in accordance with the schematic diagram shown in **Figure 2a**. Carefully weighed portions of conjugated polymer (i.e. RRe-P3HT or RRa-P3HT) were co-dissolved until fully homogenous with the elastomeric polymer (PS-PI-PS) in chloroform, which is a good solvent for all polymers involved at 50 °C 56–58. Each solution was poured over a borosilicate watch glass on top of a hot plate heated to 50 °C. The watch glasses were not treated, and no sacrificial layer was needed to ensure the samples were easily removable. The samples were then covered loosely with aluminum foil to enable a slow evaporation and allowed to fully

Soft Matter Page 10 of 51

dry (~1 hour). Films were then peeled off the watch glass with gentle steady pressure and left in a fume hood to remove any remaining solvent in the system overnight. The dry polymer blend was then heat pressed using a D16 Digital Combo Swing-Away Press from Geo Knight & Co (Brockton, MA). For the radially pressed samples, shown in **Figure 2b**, the polymers are pressed into circular steel precision shims from McMaster Carr (Elmhurst, IL) with a thickness of 254 μm and an inner diameter of 15mm at the chosen temperature. All temperatures were measured by a type-K thermocouple and recorded with an accuracy of ± 2 °C. During pressing, each sample was sandwiched between thermally conductive Kapton and two polished stainless-steel plates to create a smooth and even film. After each pressing, the film was cut, stacked, and pressed again at the same temperature. The total time for each of the three presses was 5 min, 5 min, 15 min respectively. Films were then allowed to cool slowly to room temperature over a period of 60 minutes. This repeat pressing process was used to ensure that samples were uniform and to eliminate segregation that could have occurred during drying. Films were then removed from the metal shims and stored at room temperature prior to structural measurements.

2c- Flow-Aligned Heat Pressed Sample Preparation

Processing for flow-aligned samples is shown in **Figure 2c**. These samples were arranged at one side of a rectangular shim (20.00 mm long x 2.75 mm wide x 0.45 mm high) while sandwiched between thermally conductive Kapton and two polished stainless-steel plates. All intentionally aligned samples were pressed at 250 °C. The films were also cut and stacked, ensuring the flow direction was maintained, and pressed three total times for 5 min, 5 min, 15 min, before being allowed to cool slowly to room temperature over 60 minutes. The films were then gently removed from the rectangular metal shims and stored at room temperature for

Page 11 of 51 Soft Matter

measurements. The intentionally aligned films were measured at the edge of the flow front, where the sample was forced to flow upon pressing.

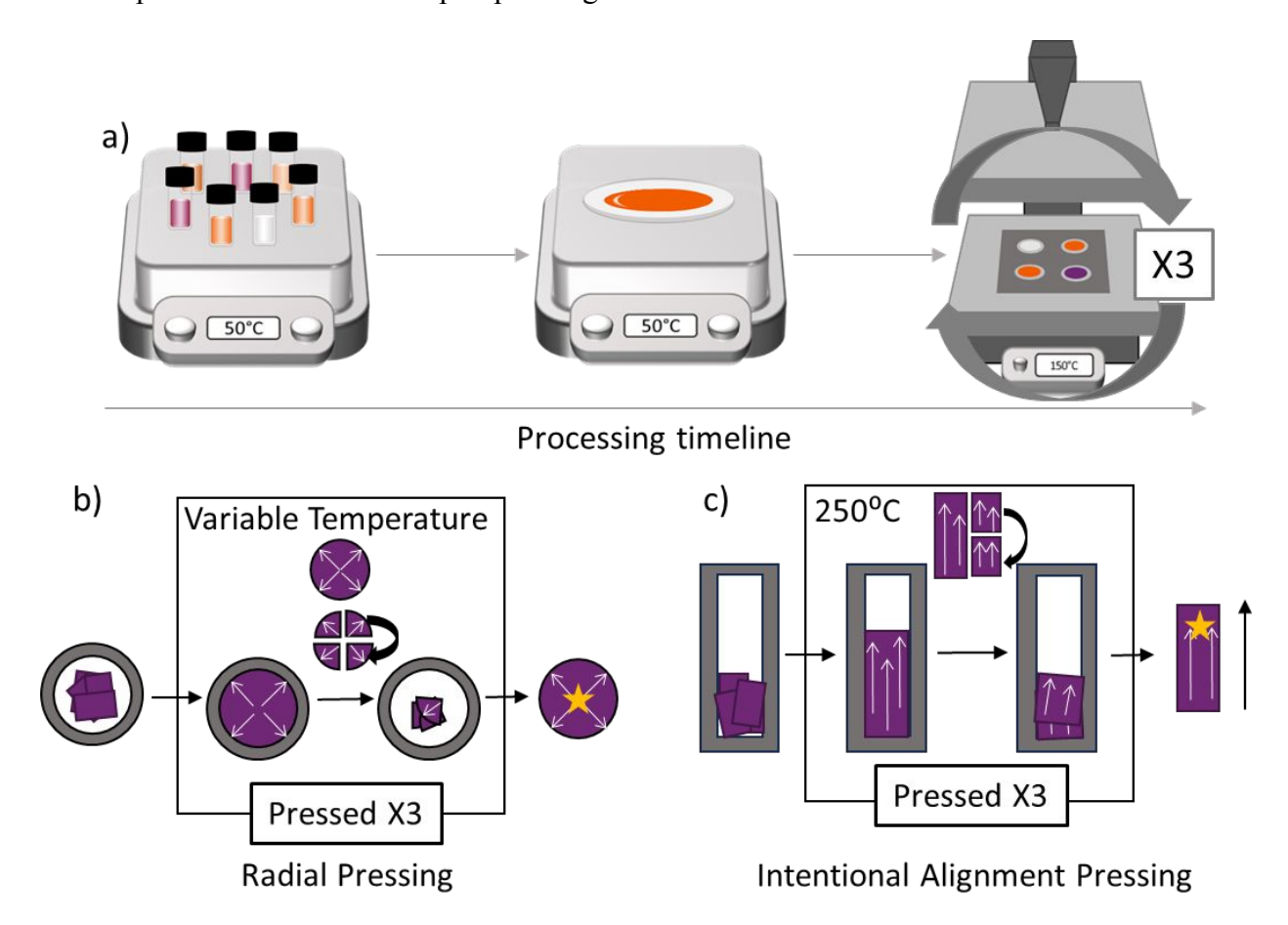


Figure 2: Schematics for sample creation for a) the full processing timeline, including codissolving of polymers into a solvent on a hotplate set at 50 °C, samples evaporating in a foil insulated watch glass until fully dry, then being pressed at a set temperature into a shim. Samples are both b) radially pressed in circular shims with samples being cut and restacked to be pressed 3 times before being measured at the starred location or c) intentionally aligned in a rectangular shim with the samples being cut and restacked with the flow direction preserved to be pressed 3 times before being measured at the starred location.

Soft Matter Page 12 of 51

2d-SANS Solution Sample Preparation

Solution samples were prepared at two different concentrations corresponding to either 5 mg/mL (low) or to a higher concentration of 10 mg/mL (high). The solvent for all samples was deuterated chloroform (dCF), which is considered a 'good' solvent for all polymers in the system^{56–58}. The lower concentration set included three samples: 5mg/mL RRe-P3HT in dCF, 5 mg/mL PS-PI-PS in dCF, and a mixed blend of 5 mg/mL RRe-P3HT and 5 mg/mL PS-PI-PS in dCF. The higher concentration set was similar with concentrations set to 10 mg/mL. The samples were prepared by carefully weighing portions of the polymers, which were then dissolved in deuterated chloroform at 50 °C in capped glass containers. For blended solutions, polymers and solvent were added at the same time and were heated until fully dissolved and homogenous. Each sample was then loaded from the hotplate into 2 mm thick quartz Hellma cells and stored at 25 °C before being measured at room temperature.

2e. Differential Scanning Calorimetry (DSC) and Thermogravimetric Analysis (TGA)

Thermophysical analysis was conducted on representative samples including the pure PS-PI-PS matrix, a blend of 5 wt% RRa-P3HT in 95 wt% PS-PI-PS, and a blend of 5 wt% RRe-P3HT in 95 wt% PS-PI-PS. Thermogravimetric Analysis (TGA) was conducted using TA instruments (New Castle, DE) Q50 Thermogravimetric Analyzer. Samples were heated at 10 °C/minute between room temperature (23 °C) and 400 °C. TGA data and analysis is provided in **Figure S4**. Differential Scanning Calorimetry (DSC) was conducted using a TA instruments (New Castle, DE) Differential Scanning Calorimeter Q200 between 0 °C and 280 °C. Samples were heated at 10 °C/minute and cooled at 5 °C/minute. Samples were weighed (PS-PI-PS – 7.9 mg, 5wt% RRe-P3HT in PS-PI-PS – 8.0 mg, 5wt% RRa-P3HT in PS-PI-PS – 5.9 mg) and run in sealed aluminum pans. A heat-cool cycle was used with three repetitions of heating and cooling to ensure any

Page 13 of 51 Soft Matter

thermal history was removed. Analysis was conducted using Python. Full DSC measurements are included in **Figure S5**.

2f. USAXS and SAXS

Ultra-small, small, and wide-angle x-ray scattering (USAXS, SAXS, and WAXS) was collected at the University of Washington using a Xenocs (Grenoble, France) Xeuss 3.0 SAXS instrument. This is a pinhole collimated laboratory SAXS instrument equipped with a copper microfocus x-ray source. Samples were collected at three sample-to-detector distances to obtain a wide Q-range. WAXS data (sample to detector distance of 0.07 m) was collected for 60 s, SAXS (sample to detector distance of 0.9 m) for 60 s, and ESAXS (sample to detector distance of 1.8 m) for 360 seconds. Samples were mounted on a 48-sample holder to enable automated processing of multiple samples. The data was reduced, averaged (except when analyzed for flow-alignment), and combined to a unified dataset that will be referred to as 'SAXS data' through this work. USAXS data was also collected using a Bonse-Hart configuration with two Si crystals, a multibounce Bartels Si(111)-crystal monochromator and a 4-bounce Si(111) crystal analyzer. USAXS was collected for two hours for each sample as well as the empty background. The sample chamber was held under vacuum at ambient temperature (approx. 20 °C) for both SAXS and USAXS measurements. Reduction of all data was performed using XSACT, the Xenocs supported software provided with the instrument, with the USAXS data being subtracted and scaled through Xenocs recommended modules. Fits and analyses were then conducted using SasView⁵⁹/sasmodels⁶⁰ and bumps⁶¹ packages for Python.

2g. Small Angle Neutron Scattering (SANS)

Small angle Neutron Scattering (SANS) measurements were collected at the Quokka beamline at the Open Pool Australian Lightwater (OPAL) source with Australian Nuclear Science Soft Matter Page 14 of 51

and Technology Organisation (ANSTO) 62 . SANS data was collected in three configurations to span the full Q range. All configurations used 5 Å \pm 0.10 Å wavelengths, with low-Q collected at 20 m sample to detector distance (2400 seconds), mid-Q collected at 12 m sample to detector distance (1200 seconds), and high-Q collected with 1.3 m sample detector distance (600 seconds). Samples were loaded into 2 mm thick quartz Hellma cells and mounted into aluminum holders placed into a temperature controlled 20 positions sample environment set to 25°C. SANS data were reduced, combined, and background subtracted using the Quokka macro in the NIST SANS package for Igor Pro 63 . Further analysis of SANS data was performed using the SasView 59 /sasmodels 60 and bumps 61 packages for Python.

2h. Scattering Data Analysis

Once fully reduced, data was exported, and further analysis was conducted using SasView⁵⁹/sasmodels⁶⁰ and bumps⁶¹ packages for Python. Features in the SAXS data were fit with shape independent models to extract structural parameters when possible.

Peaks in the SAXS region (**Figure 4**), which correspond to nanometer scale self-segregation of the block-copolymer matrix, were fit using a generalized broad peak model⁶⁴.

$$I(Q) = \frac{A}{q^n} + \frac{C}{1 + (|Q - Q_0|\xi)^m} + B$$

Here, A is the Porod scaling factor, n is the Porod exponent, C is a Lorentzian scaling factor, m is the exponent of Q, ξ is the Lorentzian screening length, and B is a flat background. Peak position is determined as Q_0 which is related to d-spacing by $Q_0 = \frac{2\pi}{d_0}$. This model does not assume any given structure (e.g. lamellar, cylindrical, cubic) and is appropriate for samples with variable ranges of order that may also result in changing phases.

Page 15 of 51 Soft Matter

Features in the USAXS region (**Figure 4**), which correspond to amorphous micron scale self-segregation of the polymers outside of the ordered nanometer scale structure, were fit using the Guinier-Porod model⁶⁵.

$$I(Q) = \begin{cases} \frac{G}{Q^s} exp \left[\frac{-Q^2 R_g^2}{3 - s} \right] & Q \le Q_1 \\ \frac{D}{Q^m} & Q \ge Q_1 \end{cases}$$

Where, s is the dimension variable to describe shape and correct the generalized Guinier law for non-elongated objects, R_g is the radius of gyration, m is the Porod exponent, G is the Guinier scale factor, and D is the Porod scale factor. The dimensional variable ranges from s=0 for globular objects, s=1 for 2D symmetry such as rods, to s=2 for 1D symmetry such as lamellae or plates. The Porod exponent describes the interface between structures, with a Porod exponent of 4 indicating a sharp and smooth interface while lower values indicate increasing roughness or intermixing between the domains. Q_1 is calculated internally through a separate equation to ensure that the derivative of each component is equal at Q_1 .

SANS data were fit using a semi-flexible cylinder model to capture free chains in solution as described by Pedersen et al⁶⁶ and which was found to be appropriate for conjugated polymers in prior works⁶⁷. Free chain fits of blends of CP and PS-PI-PS were modeled using sums of the fits for the individual components in solution. This is only appropriate when it is determined that the polymer chains are sufficiently dilute and do not have strong repulsive or associating interactions.

All analysis and modeling of the UV-VIS, DSC, USAXS, SAXS, WAXS and SANS data was performed using Python 3 (NumPy⁶⁸, pandas⁶⁹, Matplotlib⁷⁰), which aids in reproducibility, while the use of SasView⁵⁹/sasmodels⁶⁰ and bumps⁶¹ packages for Python, allows for rapid and easily adjustable fitting of the data sets.

Soft Matter Page 16 of 51

3. Results

Thermogravimetric analysis (TGA) data (**Figure S4**) shows that differences in onset of thermal decay for each sample is minimal, with the PS-PI-PS template being slightly delayed in degradation compared to the blends. A thermal decay onset of 280 °C was determined as the temperature at which 1 % of material is lost. In literature on pure and blended forms of polystyrene (PS) and polyisoprene (PI), the peak temperature for degradation is recorded around 370 °C for PI and 420 °C for PS^{71,72}. McNeill and Gupta also observed a shift in the peak degradation temperature upwards about 15 °C when the materials are mixed, due to a stabilization of each component in the blend⁷¹. Thermal degradation work has also been conducted on P3HT, with no degradation occurring until 440 °C⁷³. Thus, from our experiments and literature, all samples were processed below the degradation temperature of pure materials and their blends. In longer processing there may be exposure-dependent degradation (e.g. oxidation) that can occur, but for pressing times used in this work, the effect is expected to be minimal^{71,73}.

Differential Scanning Calorimetry (DSC) (**Figure 1f**) provides insight into the phase transitions of crystalline and amorphous regimes in each blend. The semi-crystalline regio-regular P3HT blend with PS-PI-PS shows a melting peak at 221 °C that corresponds well to the melting point of the crystalline regimes of the P3HT. This suggests that the P3HT component is still able to crystallize within these blends. There are no other distinct and obvious transitions in any of the other samples. Literature on PS-PI blends show a glass transition from the polystyrene at a temperature of approximately 85 °C, which is not observed in our samples ^{20,54}. It is possible that the DSC instrument lacks the necessary resolution to accurately measure this subtle transition, or that the PS component of these materials (22 % styrene) is too low. The published glass transition temperature for PS was still considered and set as a low end for temperatures used in processing.

Page 17 of 51 Soft Matter

SANS data collected in the solution state of these samples allows us to identify if polymers interact substantially when co-dissolved in a common solvent prior to drying.

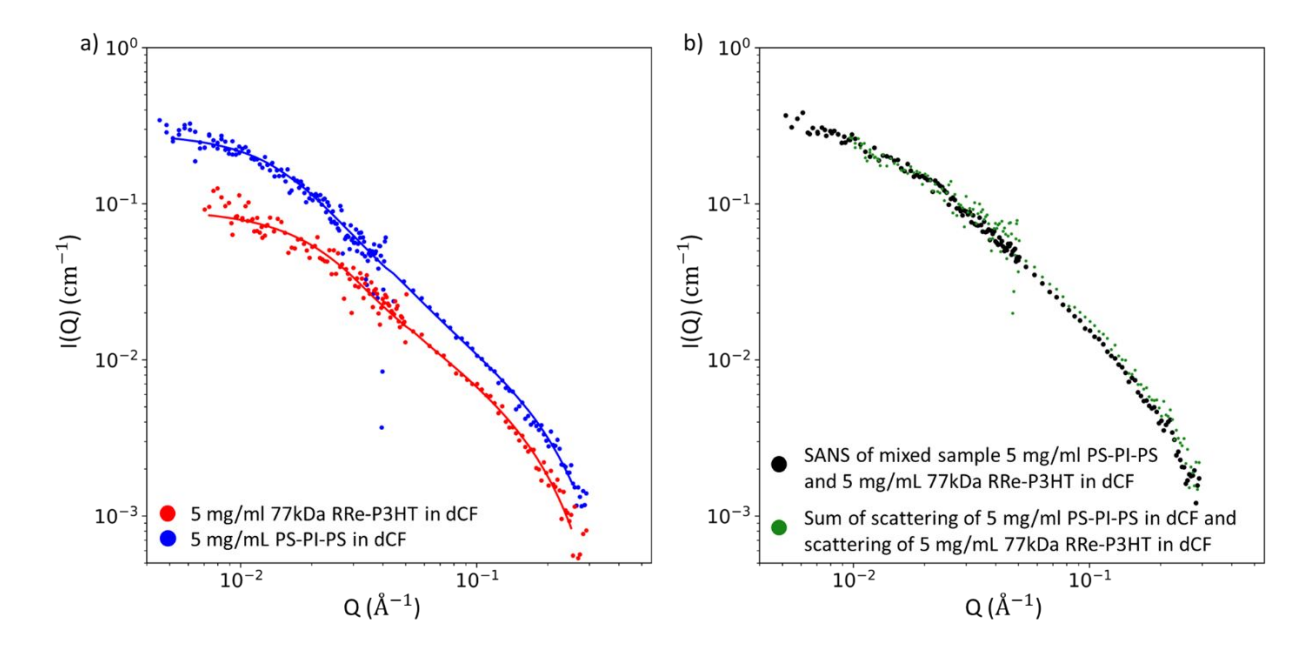


Figure 3: SANS plots of a) free polymer chains of 5 mg/ mL PS-PI-PS in chloroform-d and 5 mg/mL 77 kDa RRe-P3HT in chloroform-d. The data is fit with models of flexible cylinders which are shown with solid lines. b) SANS plot of experimentally run mixed sample of (black data points) 5 mg/mL PS-PI-PS and 5 mg/mL of 77 kDa RRe-P3HT in chloroform-d and (green data points) data of the arithmetic sum of the scattering of the individual components: 5mg/mL 77 kDa RRe-P3HT in dCF (red data in Figure 3a) and 5 mg/mL PS-PI-PS in dCF (blue data in Figure 3a).

We observe that all 'single polymer' samples (i.e. without blending) are fit well with the 'flexible cylinder' model (equations provided in SI), which describes the dimensions of a free chain in solution⁶⁶. Moreover, when polymers were co-dissolved at low concentrations, we find that the scattering intensity is nearly identical to the sum of the individual polymer components (**Figure 3b**). We interpret this as the polymers being well dissolved and not interacting substantially at low concentrations. At higher concentrations (**Figure S6**) the sum of the scattering

Soft Matter Page 18 of 51

of the individual components does not agree with the data of the experimental blend. This suggests that there is some co-assembly in solution at higher concentrations due to the interactions of the individual components. During evaporation the concentration of the cast sample will increase substantially as the solvent is removed from the system. As the concentration increases, we anticipate increased interaction and assembly between the components. Güdal et al investigated a P3HT copolymer system using in situ drying photoluminescence measurements and determined that the relative increase of polymer concentration promoted polymer chain aggregation⁴⁵. They anticipate this is due to the nucleation and crystal formation of the polymer driving further separation, resulting in large scale spinodal decomposition of components over drying⁴⁵. This insight, alongside our confirmation that P3HT and PS-PI-PS blends over 5 mg/mL display solution state crystallization, suggests that structures observed in the cast films are formed over the course of drying and are not solely a result of interactions occurring in the dilute solution state.

X-ray scattering is also performed on solid film samples after drying and processing as noted, allowing for structural information at different stages. Through the collection of ultra-small angle X-ray scattering (USAXS), small angle X-ray scattering (SAXS), and wide-angle X-ray scattering (WAXS) data, the full Q range from $3e10^{-4}\text{Å}^{-1}$ to 3 Å^{-1} is available, allowing for analysis of features from roughly ~3.2 micrometers to ~2 angstroms (**Figure 4**). Due to the weight ratio of the polymers, the self-assembled structure of the elastomer component generally dominates the signal over the sparse conjugated polymer. As the loading of conjugated polymer in the blend is changed, the structure of the elastomer matrix is modified, and this is observed in the SAXS and USAXS data. Therefore, the aggregation or segregation of the conjugated polymer within the elastomeric structure is inferred from its impact on the structure of the self-assembled elastomeric matrix.

Page 19 of 51 Soft Matter

We split the data into three regions, each covering a different scale of polymer film morphology and together covering the full scope of the impacts of the conjugated polymer additive on the structure of the elastomeric template. The low-Q USAXS region shows emerging features (i.e. a broad 'hump') with the addition of higher weight percentages of conjugated polymer (either Regio-Regular or Regio-Random) which suggest large-scale formations of phase-separated regions⁵⁰. Mid-Q features in the SAXS region are dominated by the emergence of a prominent peak around 0.018 Å⁻¹. This peak is present in all samples that are collected, including the pure PS-PI-PS matrix, and it is attributed to the characteristic spacing of the ordered structure of the PS and the PI blocks^{32,47}. From previous literature reports for this PS to PI ratio, as well as peak indexing using known Bragg Peak ratios, the phase of the pure block-copolymer matrix is identified to be hexagonally packed cylinders. With the addition of conjugated polymers, we see a characteristic peak shift and a change in shape, suggesting the cylindrical packing structure is affected by the integration of the conjugated polymer into the blend.

At high-Q (i.e. WAXS region) we observe the structure at the smallest molecular and atomic scales^{50,74}. This allows us to determine changes in the crystallinity of the components that make up the composite polymer blend. The PS-PI-PS matrix has peaks characteristic of an amorphous structure and does not display the narrow peaks that are typically attributed to polymer crystallinity. This is consistent with the elastomeric (PI) and glassy (PS) nature of the components that make up the triblock copolymer. When semi-crystalline RRe-P3HT is added, we see the emergence of two new narrow peaks that correspond to the lamellar and π -stacking peaks that are commonly observed in the literature and that allow us to track the extent of crystallinity^{50,74}.

Soft Matter Page 20 of 51

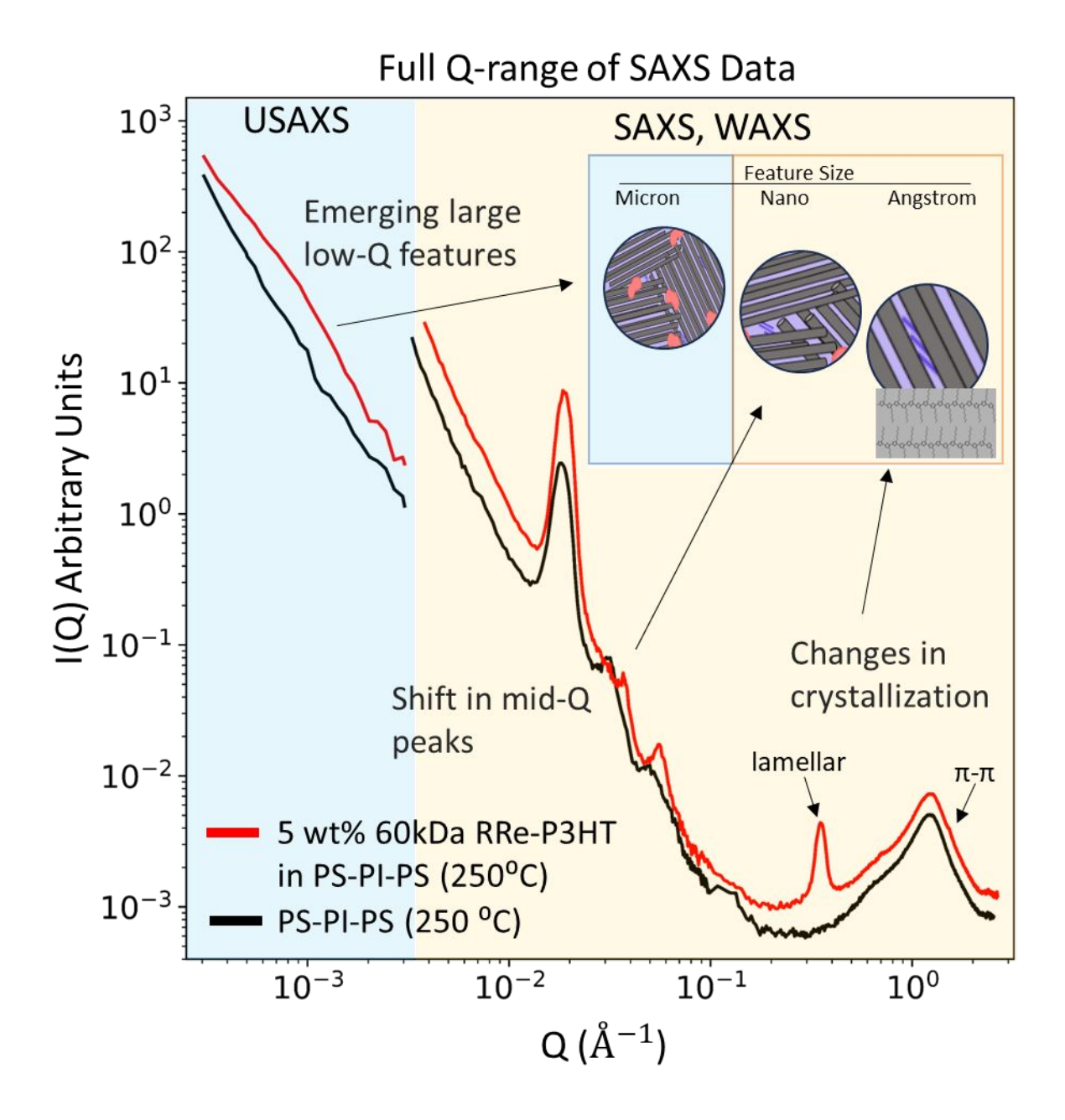
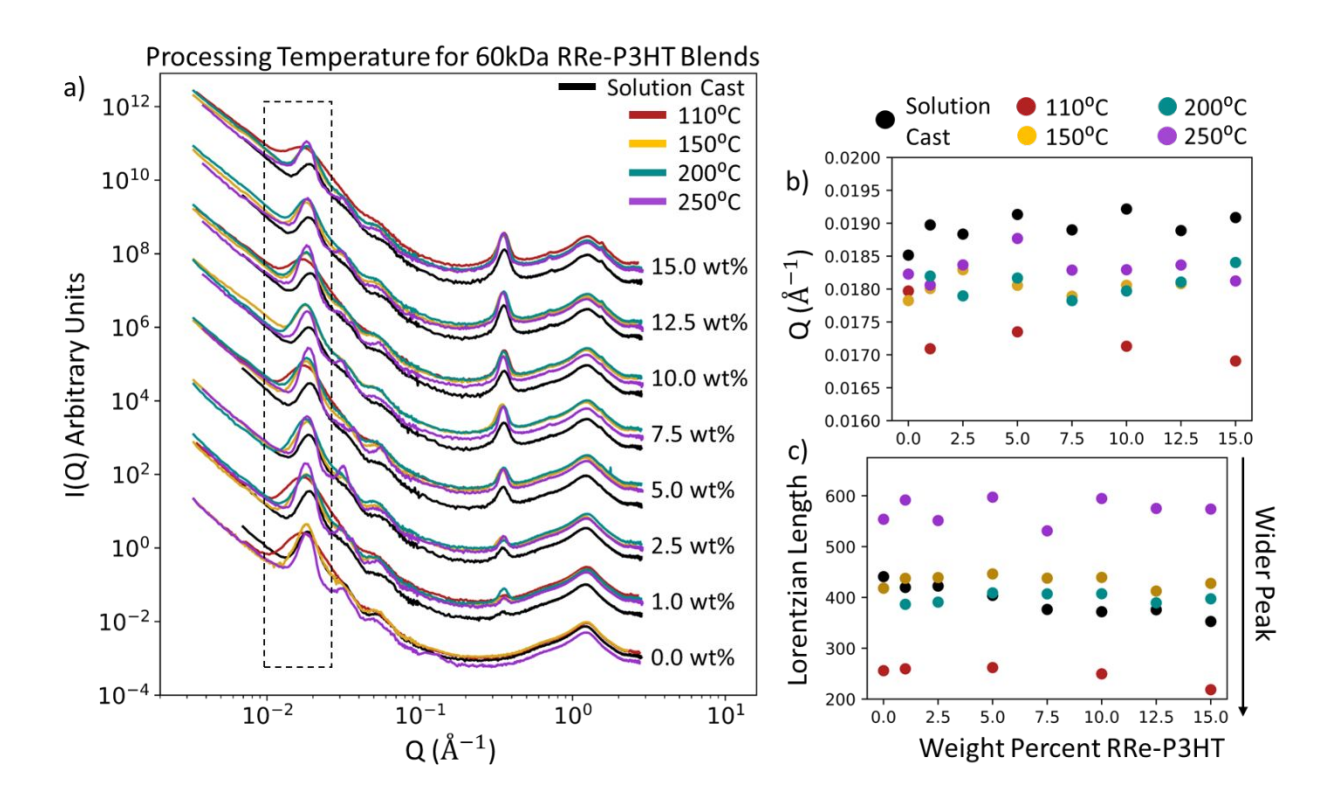


Figure 4: Full Q range of USAXS and SAXS data collected on a pure PS-PI-PS matrix sample (black) and a 5 wt% RRe-P3HT composite blend (red) from 10^{-4}Å^{-1} to 3 Å⁻¹. Peaks and features of interest have been marked and inset provide scale for each feature observed.

Blends made with the same molecular weight of RRe-P3HT are processed at different temperatures within the range of interest that is established from TGA and DSC. The temperature

Page 21 of 51 Soft Matter

change is implemented during the pressing stage of processing, with each sample being pressed for the same amount of time, but at a different temperature. Physical differences for each sample are observed, with the lowest temperature samples (pressed at 110 °C) not fully blending until the final and longest press cycle. Samples processed at these lowest temperatures showed clear physical distinctions where pieces were laid on top of each other. Some initial samples were also tested at 100 °C and these would not melt and blend even after the final long press cycle. Samples processed at intermediate temperatures (150 °C and 200 °C) are physically similar with small inhomogeneities removed in the final and longest press cycle. The highest temperature (250 °C) is completely homogenous after the first (5-minute) press cycle and is tacky when handled immediately after the press. After the final press and slow cooling, the 250 °C samples are homogeneous and physically similar to samples processed at intermediate temperatures (150 °C and 200 °C). SAXS is also collected on solution cast samples, cut from the film produced by drop casting onto the watch glasses prior to any heat pressing.



Soft Matter Page 22 of 51

Figure 5: a) SAXS data of 60 kDA RRe-P3HT and PS-PI-PS blends, labeled by wt% of RRe-P3HT added to system, and collected as cast from solution and after four different heat pressing temperatures. Data is arbitrarily shifted to separate samples by the P3HT loading in wt%. b) peak position parameters from broad peak fits of the .018 Å⁻¹ peak with colors dictated by legend above. c) Lorentzian length parameters from broad peak fits of the 0.018 Å⁻¹ peak with colors dictated by legend above.

SAXS data for these samples is collected from the Xenocs Xeuss III and spans from 0.01 $Å^{-1}$ to 3 $Å^{-1}$. Starting in the high-Q WAXS region, we can track the emergence of crystalline structures through the development of the π -stacking seen at ~1.7 $Å^{-1}$, and lamellar peaks seen at ~0.4 $Å^{-1}$. As seen in **Figure 5a**, these peaks are not visible in the fully amorphous PS-PI-PS matrix but begin to appear starting with the addition of the semi-crystalline RRe-P3HT. The lamellar peak is present in all blended samples, and the height increases as the wt% of RRe-P3HT increases. The π -stacking peak, which is known to be important for electronic performance, emerges as a very small feature in the 5 wt% RRe-P3HT sample⁷⁵. Increasing the RRe-P3HT past the 5 wt% sample, increases the height of the π -stacking peak. The presence and growth of these two peaks above 5 wt% suggest that the semi-crystalline RRe-P3HT does not significantly crystallize before this threshold. Above this concentration, it steadily increases as the weight percent of the CP increases. We do not see a large difference in WAXS peaks due to the processing temperature, suggesting that the P3HT assembly is set during the solution casting step. Which is an important finding that suggests potential manipulation of crystallization via controlled evaporation and solvent selection.

At mid-Q, we see a large peak around 0.017-0.019 Å-1 in all samples. This peak is characteristic to the PS-PI-PS template structure and by tracking changes to peak parameters, such

Page 23 of 51 Soft Matter

as location and width, we can establish how the addition of RRe-P3HT, processing, and temperature affects the phase-separated morphology^{32,47}. These peaks are fit with a broad peak model, allowing us to quantify changes as shown in Figure 5(b-c)⁶⁴. Starting with the pure PS-PI-PS, we see a large effect of the processing temperature on this peak. At 110 °C the peak is wide and as the processing temperature increases to 150 °C the peak sharpens considerably and continues to sharpen at 250 °C. This trend of increasing processing temperature to decrease peak width is maintained as RRe-P3HT is added and the wt% of the CP in the system increases. As seen in Figure 5c, the lowest processing temperatures consistently have the widest peaks, and shortest Lorentzian lengths, which is inverse to peak width. The two intermediate processing temperatures, 150 °C and 200 °C have similar peak widths, but the highest processing temperature samples display another drastic increase in Lorentzian length. This correlates to the thermodynamic thresholds established by TGA and DSC. The lowest processing temperature, which is only slightly above the T_g of the polystyrene at 95 °C -105 °C in the matrix, has the lowest levels of molecular mobility and the highest levels of disorganization in the samples. The disorganization in samples processed at 110 °C is higher than in the drop cast unprocessed samples, which we anticipate is a result of cutting and stacking during pressing without the polystyrene at a temperature that is high enough to facilitate blending. Above ~150 °C processing temperatures are well-above the Tg of the polystyrene, allowing for the glassy connections to melt and reorganize as needed. Still, blended samples may be constrained by the T_m of the RRe-P3HT at 221 ^oC and these domains may need to reorganize within the blend. The highest processing temperature is now well above the T_g of the polystyrene and is also above the T_m of the RRe-P3HT, allowing for full movement and reorganization into a thermodynamically stable structure. With these thermodynamic thresholds in mind, there is also a small shift in the peak location. Figure 5b shows

Soft Matter Page 24 of 51

a shift towards higher Q between processing temperatures of 110 0 C and 150 0 C, with no drastic trends observed with increased processing temperatures past 150 0 C. This implies that once the processing temperature is suitably above the T_{g} of polystyrene, the spacing of the reorganized structure does not change considerably with processing, only the consistency or organization of the structure.

In this Q-region, we also see a less-intense series of peaks emerge at slightly higher Q than the primary peak. Traces of these peaks are present at all temperatures, but they become clear and established at the 250 0 C processing temperature. This again suggests that there is a clear temperature dependent assembly and organization in these materials. With the emergence of secondary peaks, we can now use Bragg diffraction ratios to identify the structural phase formed by these samples and explore how they change with increasing loading of conjugated polymer additives.

Each of the peaks in the series are fitted with the broad peak model to pull the peak position and peak width metrics. These peak positions are then divided by the location of the first peak to determine the $\frac{Q}{Q^*}$ for each secondary peak. The ratios are then compared to known ratios for phase morphologies from literature to identify the sample phase. Some of the peak values do not match exactly with peaks calculated from expected ratios, especially for the peak located at ~0.05Å-1. This peak is wide and may encompass multiple peaks that have merged together due to reasons that may include limited instrumental resolution, co-existence of phases, and/or the partially disorganized nature of the samples. Best estimates are included for all peaks and ratios in **Table S1**, but a level of disorder in all the samples makes exact identification of a few peaks somewhat challenging. A selection of interest is shown in **Figure 6a** for the PS-PI-PS template material, a 5 wt% 77 kDa RRe-P3HT in PS-PI-PS blend, and a 15 wt% 77kDa RRe-P3HT in PS-PI-PS,

Page 25 of 51 Soft Matter

processed at 250 °C. For all selected samples, the peak ratios for both lamellar (solid lines) and hexagonally packed cylinders (dotted lines) are calculated from the fit peak location of the first peak. We can see the PS-PI-PS sample shows features at the expected locations for the hexagonally packed cylinders structure. As seen in **Figure 6b**, when RRe-P3HT is added into the system at low amounts, 1 wt% and 2.5 wt%, there are no major changes in peak locations or ratios and the hexagonally packed cylinder phase is maintained. At 5 wt% the peak in the ~0.03 Å-1 range disappears, leaving a ratio that is more indicative of the formation of a lamellar phase [1.0, 2.0, 3.0]. As more conjugated polymer is added into the system the peak in the ~0.03 Å-1 range remerges and the 7.5 wt%, 10 wt%, and 12.5 wt% samples show a mixture of disordered hexagonally packed cylinder peaks and lamellar peaks. There is a clear peak in the ~0.03 Å-1 range, which equates to the ~1.7 ratio, but the peak in the ~0.05 Å-1 range is wide enough that it encompasses the locations for both the 2.65 and 3.0 ratios. At the maximum loading of 15 wt% RRe-P3HT in PS-PI-PS, we see a return to the hexagonally packed cylinder ratios, and also a return to similar levels of order as seen in the pure template.

Soft Matter Page 26 of 51

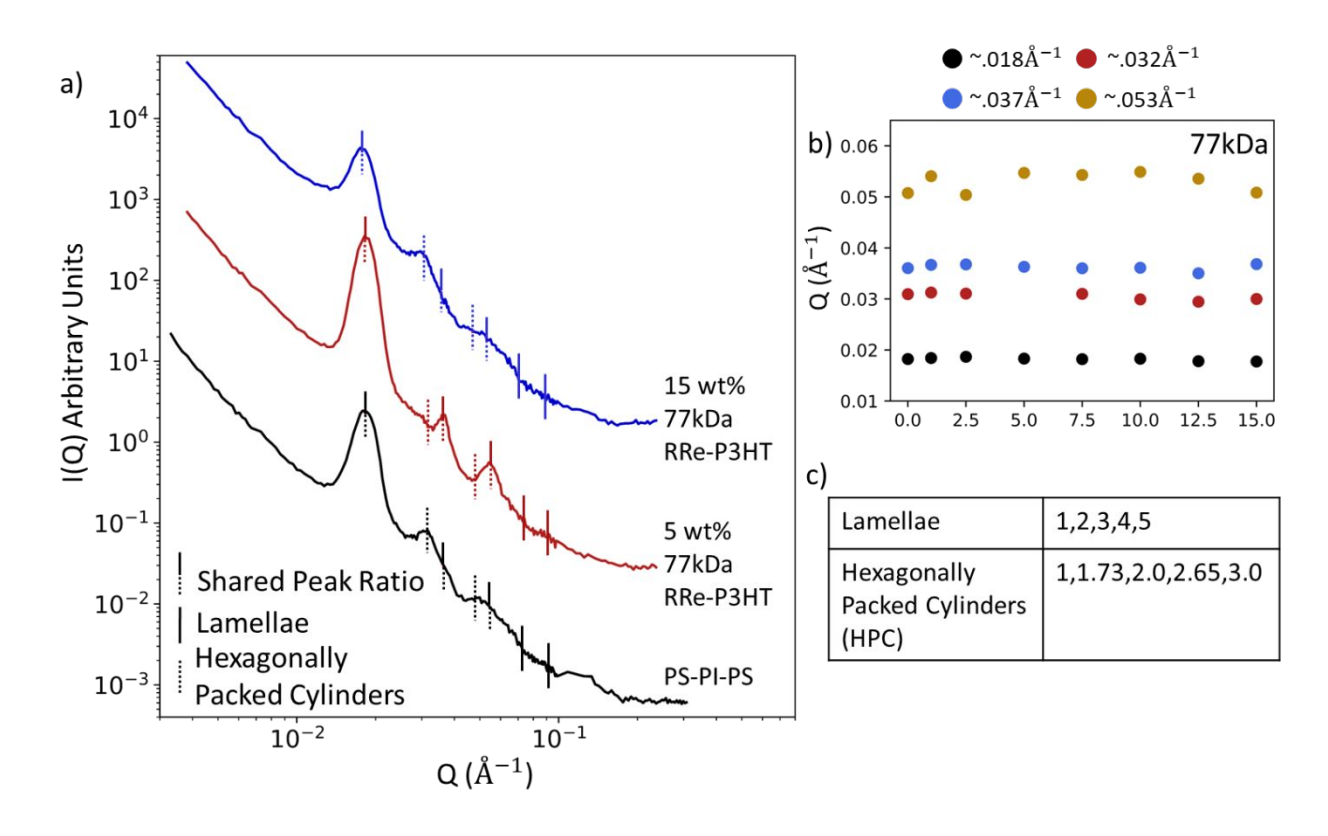


Figure 6: a) SAXS data of selected 77 kDA RRe-P3HT and PS-PI-PS blends, labeled by wt% of RRe-P3HT added to system, and collected at 250 °C. Lines are added to mark where peaks are expected for lamellar and hexagonally packed cylinder structures. Locations where peak ratios overlap are depicted with both solid and dotted lines. Data is arbitrarily shifted to separate samples into wt%. b) peak position parameters from broad peak fits of all peaks with colors dictated by legend above. c) ratio of peaks for lamellar and hexagonally packed cylinders from the main peak q*.

Alongside processing temperature changes, we ran a series of samples with changed RRe-P3HT lots with low (42 kDa), medium (60 kDa), and high (77 kDa) molecular weights. These samples were all processed identically, with the only change being the RRe-P3HT molecular weight. When heat pressed at a processing temperature of 150 °C, as seen in **Figure 7**, we see no

Page 27 of 51 Soft Matter

significant difference between the samples with differing molecular weights. Slight differences in low-Q can be observed at 7.5 wt% and up, but the peaks do not change considerably. Parameters of these ~0.018 Å⁻¹ broad peak fits can be seen in **Figure 7b** and **Figure 7c**. We see slight fluctuations in the peak location at wt% above 7.5, but the differences observed are not significant. Small fluctuations are also seen in the Lorentzian length, but again, none of these changes are indicative of impact.

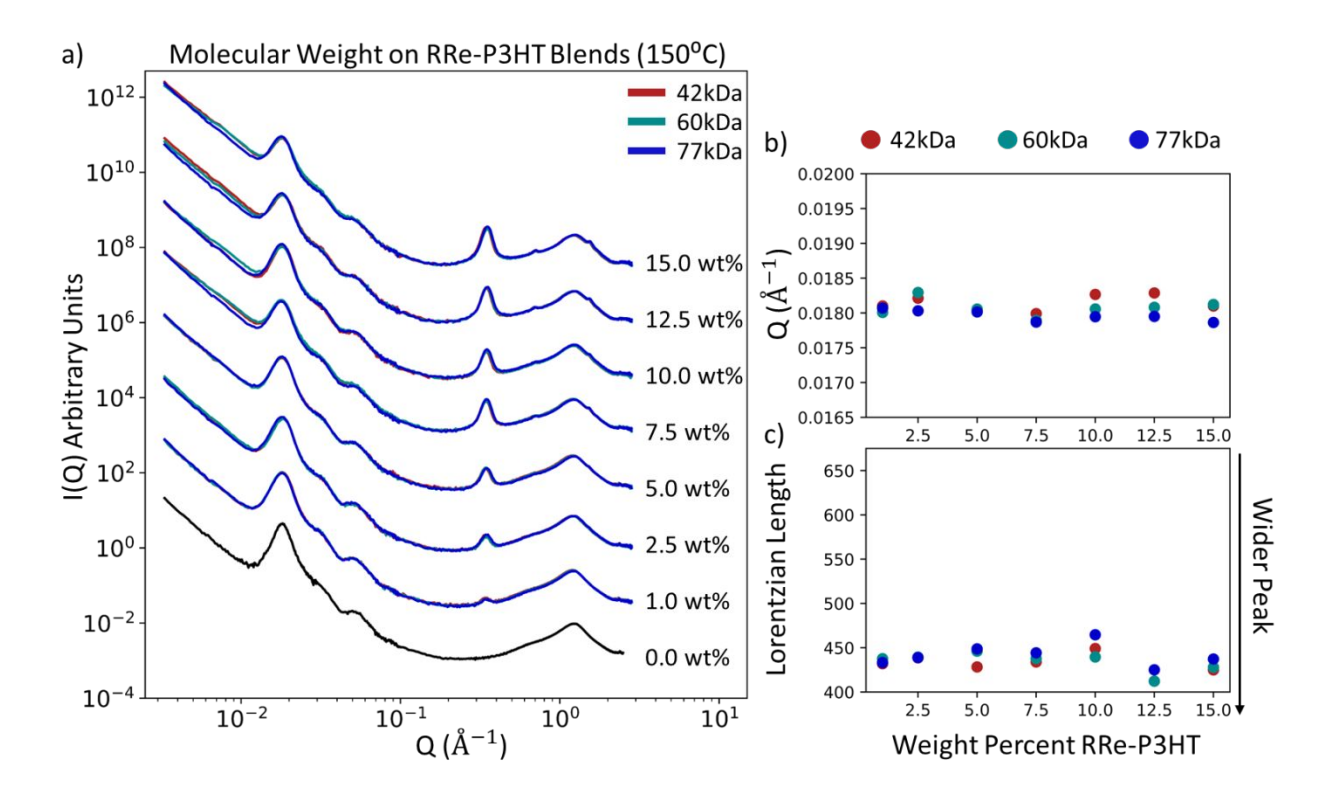


Figure 7: a) SAXS data for blends of RRe-P3HT and PS-PI-PS, corresponding to three different molecular weights and labeled by wt% of RRe-P3HT added to system. All samples are collected at 150 °C. Data is arbitrarily shifted to separate samples by wt%. A zoomed in focus on the peak range of interest is provided in **Figure S10a**. b) peak position parameters from broad peak fits of the .018 Å⁻¹ peak with colors dictated by legend above. c) Lorentzian length parameters from broad peak fits of the .018 Å⁻¹ peak with colors dictated by legend above.

Soft Matter Page 28 of 51

Identical samples are also processed at 250 °C, with increased observed differences between the temperature series. As seen in Figure 8a, by increasing the temperature of processing there is more variation in the location, width, and prevalence of secondary peaks in the region of interest. There is a clear variability in the peaks between molecular weights of RRe-P3HT as the loading increases. This variability is maintained even within replicates of the same molecular weight as seen in Figure S9. We anticipate that the higher processing temperature makes samples more sensitive to processing changes, leading to slight variations in the onset, extent, and trends of phase and order. This variation is present across molecular weights, and we anticipate that any changes that are caused by the increasing molecular weight of P3HT are disguised within the sample sensitivity. While these variations prevent any concrete analysis of the effect of molecular weight, we can observe general trends as the weight percent increases in each series. At intermediate loadings (2.5 - 10.0 wt%) we again see a peak at ~0.03 Å⁻¹ disappear for all molecular weights and an increase in the prominence of the peak at ~0.04 Å⁻¹. By 10 wt% RRe-P3HT, we see the 0.03 Å⁻¹ peak reappear for all samples. At the highest loadings of RRe-P3HT (12.5-15 wt%) the peaks widen significantly, indicating increased disorder, and differences between molecular weights of RRe-P3HT is greatly reduced. This is mirrored in the replicates shown in Figure S9, with all samples showing a peak shift between 2.5 wt% and 10 wt% and the variation between samples reduced for low (1 wt%) and high (>12.5 wt%) loadings of RRe-P3HT.

The primary peak at 0.018 Å⁻¹ is again fit with a broad peak model and selected series of parameters are extracted and shown in **Figure 8(b-g)**. Due to the processing sensitivity in the midwt% range drawing explicit trends is difficult, but a few general observations were made. Through all the replicates, the 77 kDa RRe-P3HT samples trended at a higher Lorentzian length, or narrower

Page 29 of 51 Soft Matter

peak. This suggests that there is a slightly more ordered structure forming in the highest molecular weight series. The 42 kDA RRe-P3HT series showed the highest consistent peak locations, suggesting that spacing between the phase-separated segments in the template is slightly smaller for the lowest molecular weight CP additive.

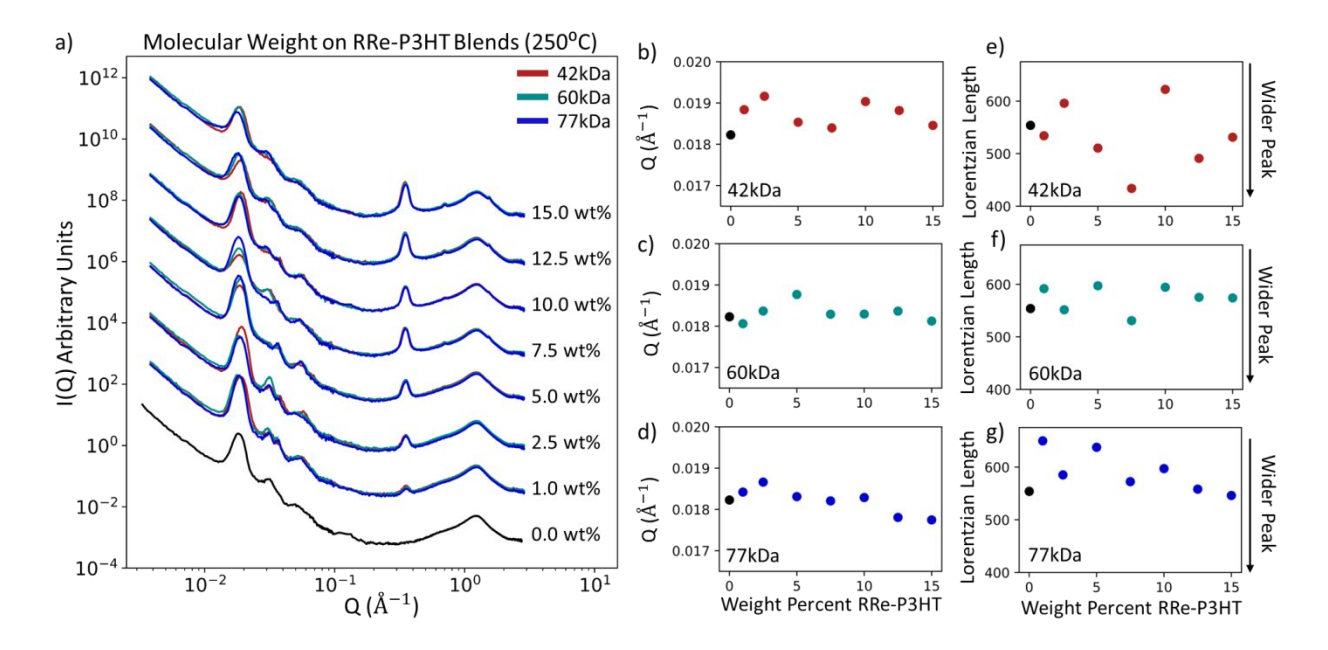


Figure 8: a) SAXS data of RRe-P3HT and PS-PI-PS blends corresponding to three different molecular weights and loadings. All samples were heat pressed at a temperature of 250 °C. Data is arbitrarily shifted to separate samples by P3HT loading. A zoomed in focus on the peak range of interest is provided in **Figure S10b**. b-d) peak position parameters from broad peak fits of the .018Å-1 peak separated by molecular weight of RRe-P3HT. e-g) Lorentzian length parameters from broad peak fits of the 0.018 Å-1 peak separated by molecular weight of RRe-P3HT.

The impact of P3HT molecular weight on the phase of the matrix was also examined. As noted before, adding 77 kDa RRe-P3HT causes a phase shift from hexagonal cylinders (pure PS-PI-PS and low wt% loadings) to a mixed phase and a lamellar structure (5 wt% RRe-P3HT), and finally to a mixed phase with increasing hexagonal cylinder components at higher loadings. Phase analysis was also conducted for blends with 42 kDa RRe-P3HT and 60 kDa RRe-P3HT and similar

Soft Matter Page 30 of 51

results are found, as shown in **Figure S8.** All peak ratios and phase determinations for all molecular weights are shown in **Table S1**.

Changes are also observed in the low-Q feature that is observed in the USAXS regime for blend samples. Solo samples were measured then rotated 90° then measured again to ensure that any USAXS feature was not dependent on changes in alignment direction of samples (Figure S11). Measured samples shown here were stacked three times thick to ensure scattering signal-tonoise was good for analysis. As seen in Figure 9a, the pure PS-PI-PS matrix does not display any significant features in this length scale, beyond the power-law scaling of -2.6. This data collects low-Q data of large-scale features, and data overlap with the main peak of interest discussed in the SAXS data can be seen in the high-Q of **Figure 9a**. With the addition of semi-crystalline 60 kDa RRe-P3HT at concentrations of 1 wt% there is no significant change in the shape or intensity of the data. At 5 wt% RRe-P3HT, a feature or 'bump' emerges in the 0.0005 Å⁻¹ - 0.001 Å⁻¹ region that is indicative of phase separation at micrometer length-scales. As the conjugated polymer concentration is increased, the intensity increases and the feature shifts further towards lower Q, indicating that feature is growing in size. At the highest wt% measured, the feature is absent, and we anticipate that the size of the phase separated regions has grown outside of the length scale of our instrument. The emergence of the feature at 5 wt% conjugated polymer corresponds to phase shift that is observed in the SAXS regime (Figure 8). This feature is fit with a Guinier-Porod model. This is a shape independent model that combines size-based parameters associated with a Guinier turnover and interfacial analysis through fitting the Porod exponent. Only the 5 wt% and the 10 wt% RRe-P3HT blends show features in the length scale we investigated, and are the only samples fit with this model. A metric of size, the radius of gyration, is shown in Figure 9c plotted against weight percent of RRe-P3HT added into the system. When the structure is formed at 5

Page 31 of 51 Soft Matter

wt% RRe-P3HT, it is about 360 Å and at higher conjugated polymer weight percents the structures grow larger. This trend continues until it falls out of the range of measurement for the instrument's resolution, but we anticipate that this trend continues as further conjugated polymer is added. The Porod exponent, observed in Figure 9d, describes the interface between the RRe-P3HT amorphous structures and the surrounding PS-PI-PS. Both weight percents that were fit have a Porod exponent of about 4, which describes smooth and sharp interfaces between domains. When processed at lower temperatures, shown in **Figure S12a**, the trend remains, but the intensity and clarity of the feature is reduced. We also see the growth of the feature out of our attainable length scales around the 10 wt% sample, earlier than we see in the 250 °C series.

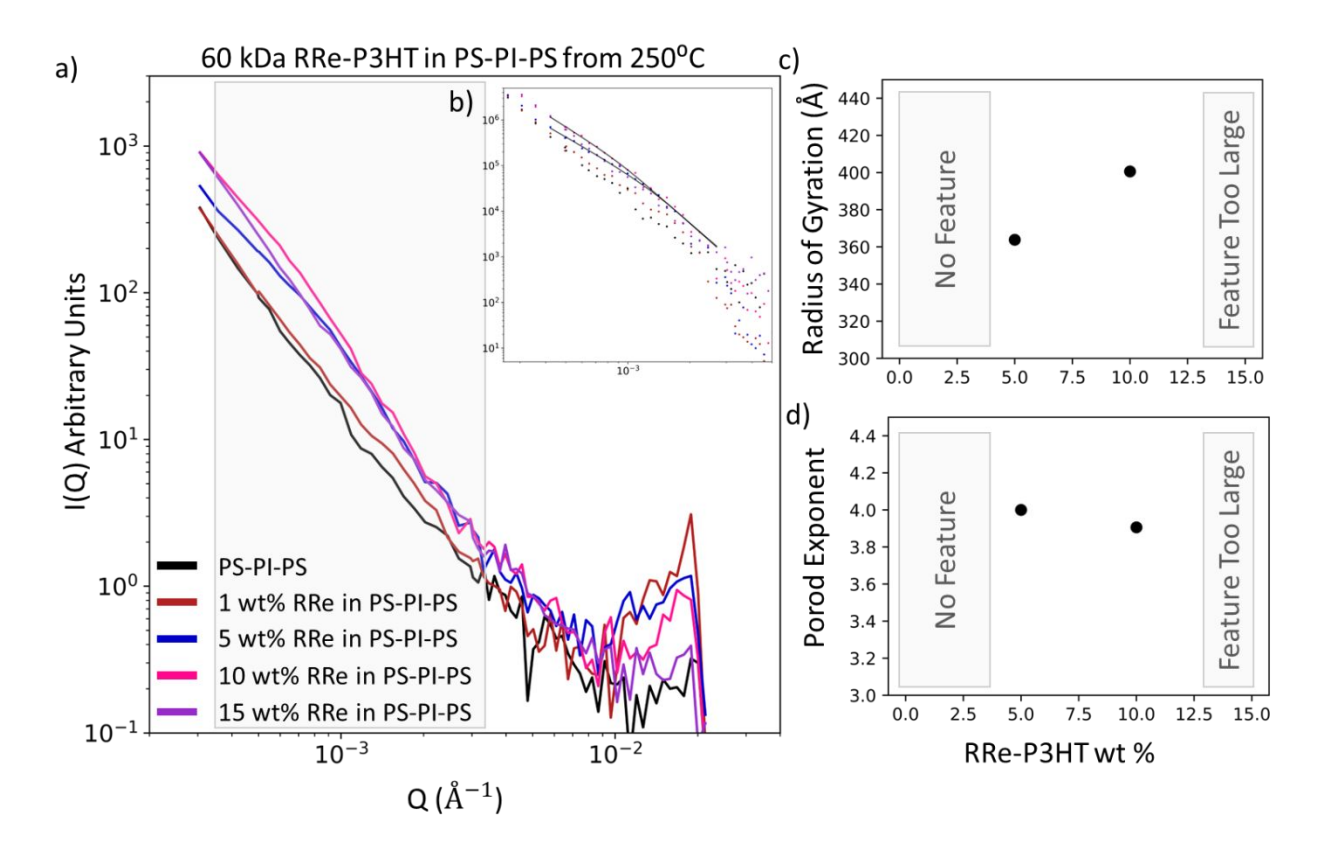


Figure 9: a) Smeared USAXS low-Q data of 60 kDa RRe-P3HT and PS-PI-PS blends processed at 250 °C with region of interest marked in grey b) zoom of region of interest of low-Q region of desmeared USAXS data of 60 kDa RRe-P3HT and PS-PI-PS blends processed at 250 °C with

Soft Matter Page 32 of 51

Guinier-Porod fits. Data points are plotted as points and Guinier-Porod fits are plotted using black lines. Guinier-Porod fit parameters for 60 kDa RRe-P3HT were extracted and c) radius of gyration and d) Porod exponent is plotted against weight percent of conjugated polymer added.

Experiments were also repeated using an amorphous regio-random P3HT (RRa-P3HT) to evaluate the effect regio-regularity and P3HT crystallization on the composite structure. Samples were processed, measured, and analyzed in the same way as previously outlined for RRe-P3HT, with samples processed at 110, 150, and 250 °C. SAXS measurements are discussed here, but USAXS measurements are available in Figure S12c and discussed further in the supplemental information. Figure 10a shows a peak at 0.018 Å-1 and similar trends to those observed for RRe-P3HT samples in **Figure 5**. We again observe a wide primary peak that sharpens as the processing temperature increases from 110 °C to 250 °C. The Lorentzian length parameters (Figure 10c) corroborates this observation, with each increase in temperature leading to sharper peaks and more order in the system. There is more variation in peaks parameters, both location (Figure 10b) and width, for 63 kDa RRa-P3HT than observed with its semi-crystalline counterpart of 60 kDa RRe-P3HT. When peak indexing and phase identification is performed on the 250 °C RRa-P3HT samples, we see the same trend observed with the RRe-P3HT samples. The pure PS-PI-PS is identical to the one used in the RRe-P3HT blends and is identified as hexagonally packed cylinders. As small amounts of RRa-P3HT (1 wt%) are added into the blend, peaks sharpen, and the phase is maintained as hexagonally packed cylinders. At a loading of ~5 wt% RRa-P3HT, the peak at ~0.032 Å-1 disappears and a peak at ~0.037 Å-1 emerges, consistent with a lamellar. At high loadings of RRa-P3HT, the peaks widen, and the ratios return again towards hexagonally packed cylinder phases. Fits and ratios for phase identification can be seen in Figure S13.

Page 33 of 51 Soft Matter

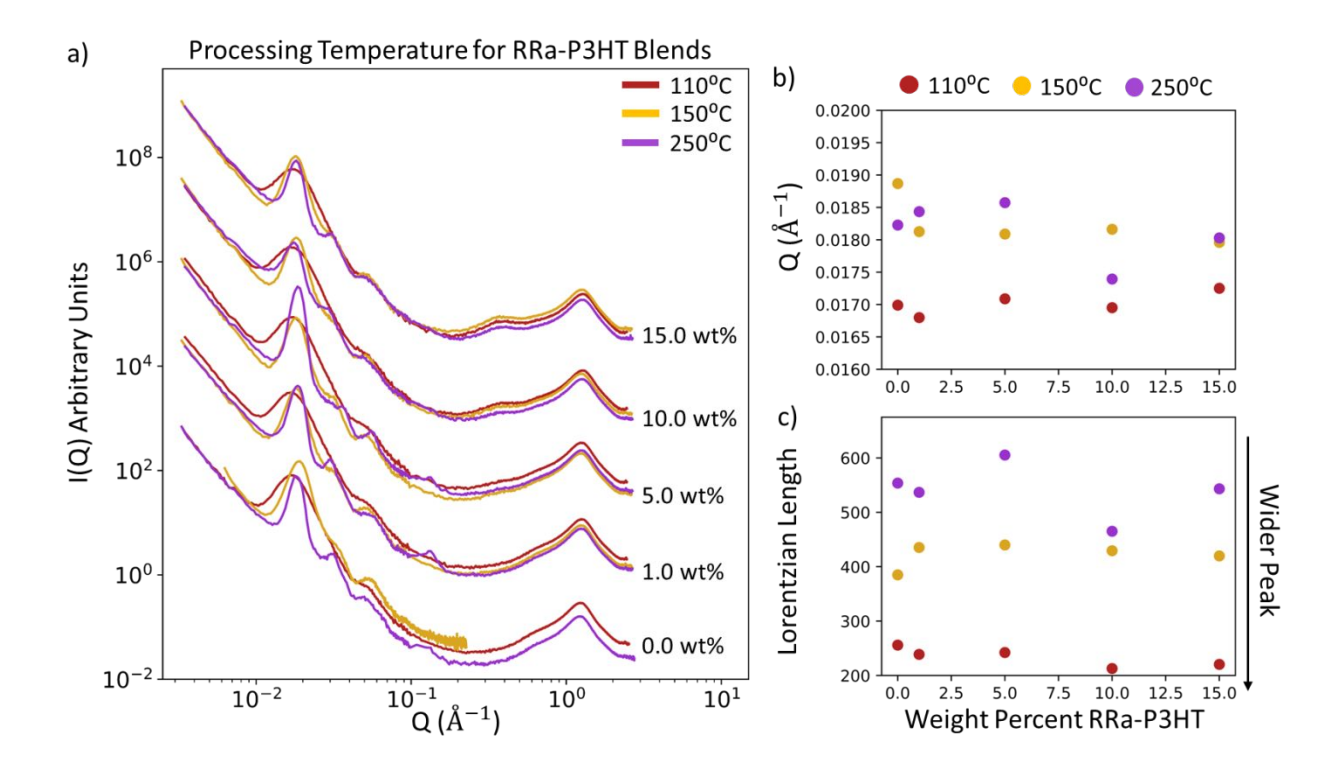


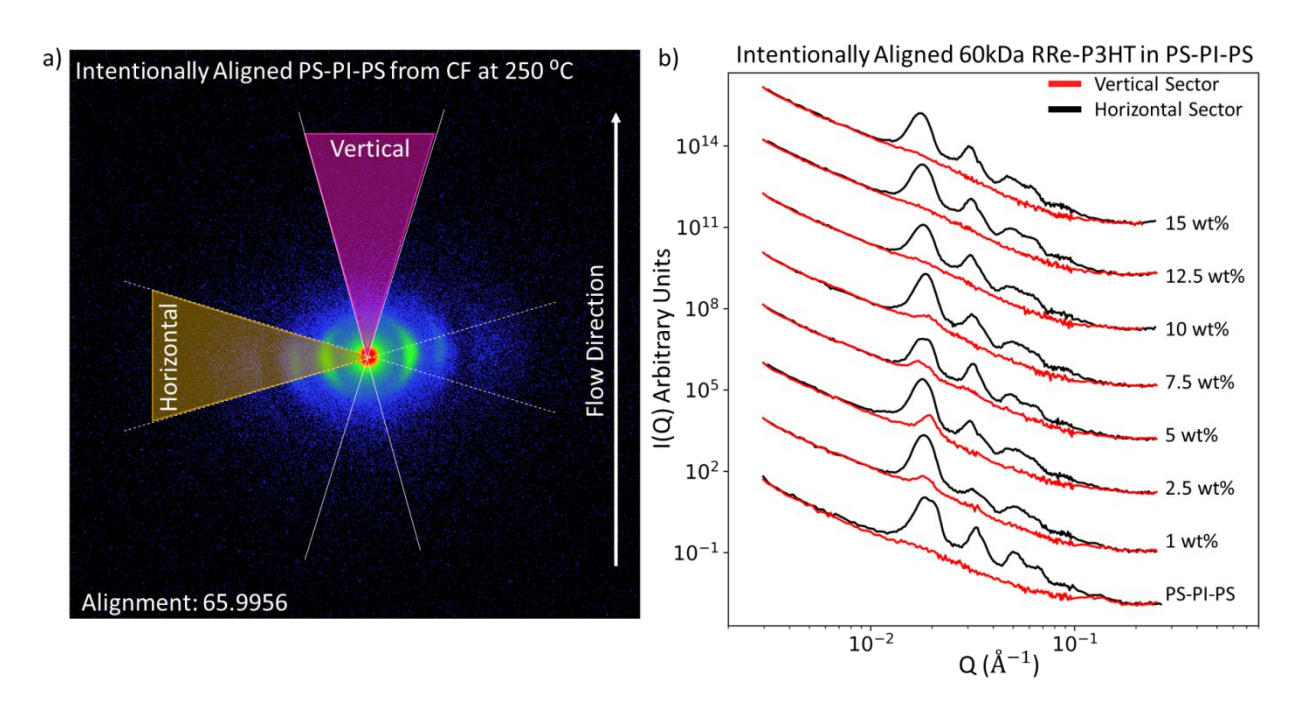
Figure 10: a) SAXS data of 63 kDA RRa-P3HT and PS-PI-PS blends, labeled by wt% of RRa-P3HT added to system, and collected at three different heat pressing temperatures. Data is arbitrarily shifted to separate samples by P3HT loading. b) peak position parameters from broad peak fits of the .018 Å⁻¹ peak with colors dictated by legend above. c) Lorentzian length parameters from broad peak fits of the .018 Å⁻¹ peak with colors dictated by legend above.

The processing methods used in all previously discussed samples utilized a circular mold with cutting and folding between pressings to minimize flow-alignment that can occur as samples spread from the center of the shim. Still, flow can vary from sample to sample and press to press without a way to carefully control, repeat, or facilitate the movement. To check on the impact of flow, we also prepared a subset of samples in a rectangular shim to intentionally align the structure by forcing the sample to flow in a set direction during processing. The flow pattern was maintained

Soft Matter Page 34 of 51

over each press and the structure was measured using SAXS at the flow front. For this data set we refer to the direction of flow as "vertical" and the direction orthogonal to flow as "horizontal".

The conversion to 1D data for the intentionally aligned sample was done by sector averaging, with a 30° slice of the image chosen to average Q values. As shown in **Figure 11a**, two sections were chosen for the averaging, the first was horizontal to capture the highest intensity regions and the second was vertical to capture the lowest intensity regions. The two regions allow for an understanding of the 1D peak information in the flow direction and the structures that are not flow aligned. In the 1D plot, **Figure 11b**, we can see that see that the pure PS-PI-PS and the higher weight percent blends (>10 wt% RRe-P3HT) have no scattering features or peaks in the vertical sector, which is a sign of excellent flow-alignment. At intermediate loadings (1 to 7.5 wt% RRe-P3HT), scattering features are observed in the vertical sector with a peak around 0.018 Å-¹. Still, secondary peaks that are clearly visible in the horizontal sector are not observed in the vertical sector data of samples. When indexed as shown in **Figure S14**, flow-aligned samples all were identified as hexagonally packed cylinders at all concentrations.



Page 35 of 51 Soft Matter

Figure 11: a) 2D images from 0.9 m SAXS runs for flow-aligned PS-PI-PS cast from chloroform and processed at 250 °C with overlays on the sectors radially averaged for the horizontal and vertical directions b) Vertical and horizontal integrated SAXS data for 60 kDA RRe-P3HT and PS-PI-PS blends, as a function of RRe-P3HT loading. Data is arbitrarily shifted vertically for clarity.

In 2D detector images (i.e. no radial averaging), samples showed clear signs of alignment that were not as evident in radially pressed samples. In **Figure 12**, we see that radially processed samples (**Figure 12b**) show low alignment factors and more isotropic scattering patterns with one highly visible ring correlating to the main peak in the data. In contrast, for intentionally aligned samples (**Figure 12a**) the ring develops into spots of high horizontal intensity that correlates well with the vertical flow direction. We also observe a sizable increase in the alignment factor from 0 (isotropic) to 100 (perfectly aligned), between the radially pressed and intentionally aligned samples. Calculations for the alignment factor are done in the XSACT software (Xenocs) that extracts alignment parameters from a tensor approach, for which equations and tensors are provided in the Supplemental Information. We especially see this increase in alignment in pure PS-PI-PS and in blends with higher loadings of RRe-P3HT (10-15 wt%) blends. The 2D scattering patterns in **Figure 12** help to demonstrate that shear alignment is possible but also strongly dependent on the composition and loading of the blends.

Soft Matter Page 36 of 51

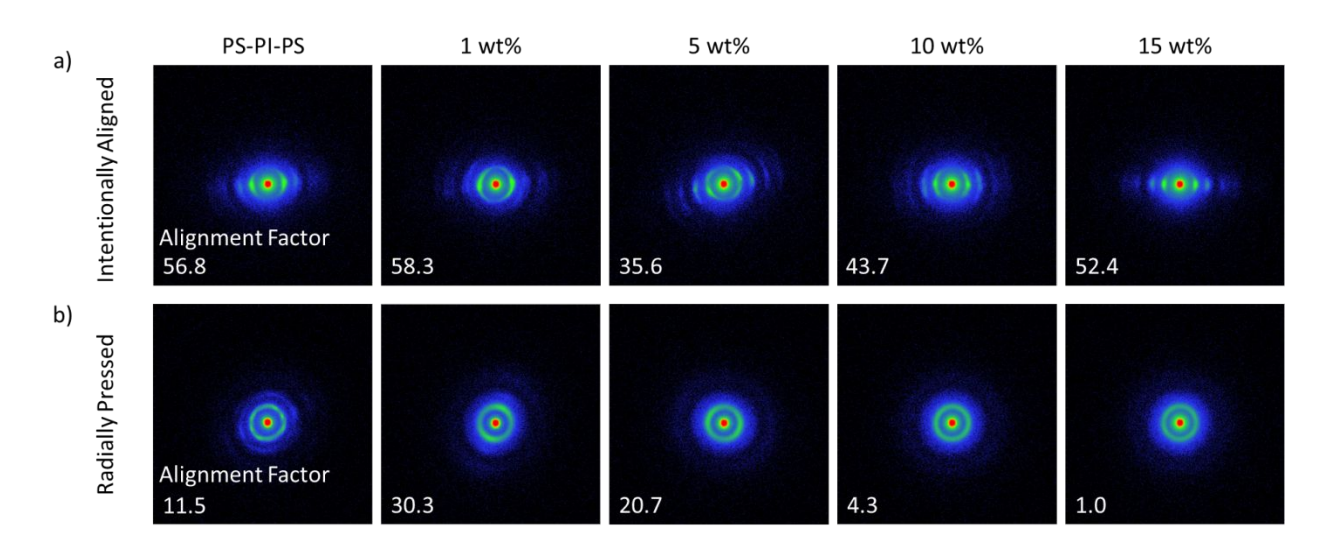


Figure 12: 2D images from 0.9 m SAXS runs for a) intentionally aligned samples and b) radially pressed samples of pure, and 60 kDa RRe-P3HT and PS-PI-PS blended systems, processed at 250 °C, denoted by the weight percent of additive in the mixture. Alignment factors are included for all samples and characterize the extent of alignment, with 0 being isotropic and 100 being maximally aligned.

4. Discussion

We were able to determine that the processing temperature of a polymeric blend has a large impact on the morphology, specifically the extent of organization of the elastomer matrix. In dilute solution states, seen at low concentrations, we do not see any assembly in blends, and the structures observed are described well by free chains of the individual components (**Figure 3**). As the concentration of the polymers in solution increases, we see scattering in the blended sample that is indicative of complexation. Due to this, we know the structures observed in the solid forms are formed over the course of evaporation as concentrations increase and are not a result of interactions while in dilute solution states. During solution casting, structures are largely determined by kinetic

Page 37 of 51 Soft Matter

effects of solvent evaporation and the arrest of molecular motions. This is generally insufficient to create clear domain segregation and long-range structural assembly.

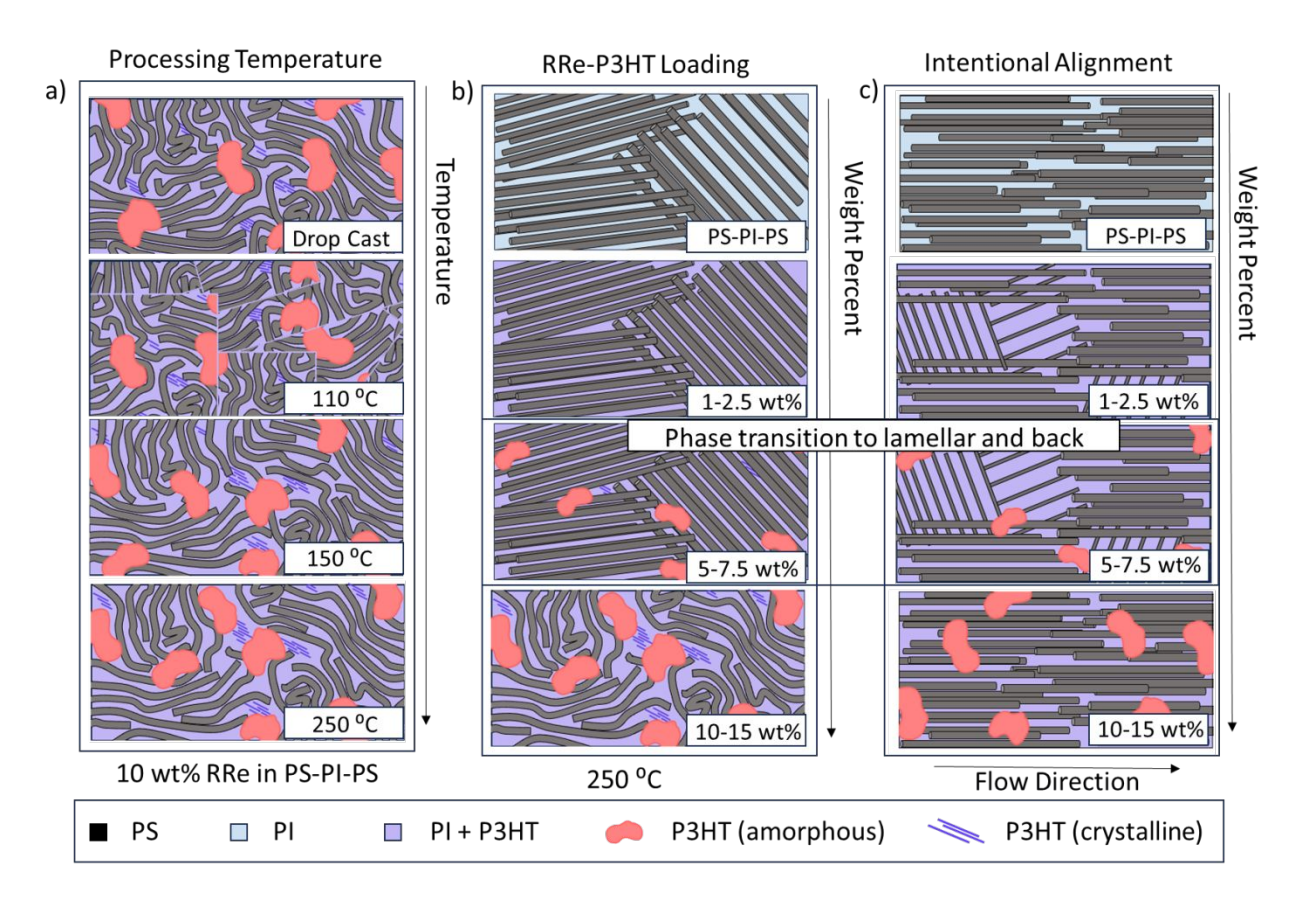


Figure 13: Schematic describing the morphology of RRe-P3HT and PS-PI-PS blends as a) 10 wt% RRe-P3HT is processed at varying temperatures b) RRe-P3HT is added in increasing weight percent to PS-PI-PS, processed at 250 °C and c) intentionally aligned samples of RRe-P3HT and PS-PI-PS with increasing amounts of RRe-P3HT

As seen in **Figure 5** and described in **Figure 13a**, when processed at low temperatures (110 0 C) the glass transition temperature of the glassy polystyrene (95-105 0 C) is barely surpassed and does not provide the required energy or time that is needed to further segregate and assemble. This results in a disordered structure that is difficult to identify due to the lack of organized diffraction peaks. Additionally, the cutting and stacking throughout processing without the temperature

Soft Matter Page 38 of 51

necessary to allow the PS to be rearranged, leads to more disorder than the solvent-cast analogue sample. Higher temperatures facilitate the incorporation of P3HT into the structure of the PS-PI-PS and allow for the system to assemble and order fully. We see improvements in order at the intermediate temperatures (150 and 200 °C) where the structure becomes more organized and regular. However, when processing at 250 °C we see the greatest increases in ordering as well as the clarification of phase structures (i.e. close-packed hexagonal cylinders and lamellar phases) due to the emergence of higher-order diffraction peaks.

We identify the phase of pure PS-PI-PS as hexagonally packed cylinders, consisting of cylinders of polystyrene assembled within a matrix of polyisoprene (**Figure 6**). This is consistent with the material architecture and phase-diagrams outlined in the literature³⁰. With the addition of RRe-P3HT to the blend, there are evident changes to the morphology of the matrix as a function of concentration (**Figure 6**). We anticipate that P3HT incorporation occurs primarily in the polyisoprene domains due to the more favorable Flory interaction coefficient between P3HT and PI, which is estimated between 0.02 and 0.23^{51,53,76}. The Flory interaction coefficient between PS and P3HT, which is estimated at 0.48, favors phase separation and previous neutron scattering work indeed demonstrated the large-scale phase segregation of P3HT and PS^{50,77}.

As shown in **Figure 13b**, the order and regularity in the system increases at low loadings of conjugated polymer in the blend system. At ~5 wt% loading of RRe-P3HT in PS-PI-PS, a gradual shift occurs from a hexagonally packed cylinder phase to a lamellar-rich phase. Indexing this phase shift over a series of intermediate loadings (2.5 - 10 wt%) is challenging due to these phases coexisting over a broad range. Still, a clear loss of hexagonally packed cylinder peaks for the 5 wt% sample signals a lamellar phase dominated material at this point (**Figure 6**). We also anticipate that 5 wt% marks a critical concentration where large-scale segregation of P3HT-rich

Page 39 of 51 Soft Matter

domains emerges, this is confirmed in the appearance of the low-Q feature seen in the USAXS data in **Figure 9.**

Increasing concentration past this loading again changes the bulk of the matrix phase from lamellar-rich to hexagonal cylinders. At 7.5 wt% and 10 wt% RRe-P3HT, key peaks for hexagonally packed cylinders reemerge but disorder is increasingly present in the system as noted by the reduced sharpness of the peaks. At the highest loadings (12.5 and 15 wt%) we observe an increase in peak widths indicating an overloading of conjugated polymer in the system leading to increasing disorder in the arrangement of the cylinders and the increase in size of phase-separated RRe-P3HT domains (**Figure 9**). This suggests that there is a critical concentration around 5 wt% where there are significant changes in the morphology while incorporating into the PS-PI-PS templated structure, as well as a secondary concentration where disorder increases between 10 wt% and 12.5 wt% RRe-P3HT.

Increased processing temperature also allows us to identify the effect of molecular weight of the RRe-P3HT additive on the structure of the blends. When processed at 150 °C, there is no significant change between the sample series, and it appears that the molecular weight does not have an impact on the blend structure (**Figure 7**). When processed at 250 °C, there are minor differences between sample series and the effect of molecular weight of RRe-P3HT on blend morphology can be identified (**Figure 8**). These differences are minimized due to the increase in processing sensitivity of these samples at higher temperatures identified in replicates of the same molecular weight (**Figure 89**). This sensitivity is highest for samples in the 2.5 -10 wt% range, where phase transitions are identified for all P3HT blends with all molecular weights (**Figure S8**) as well as with amorphous RRa-P3HT (**Figure S13**). So regardless of the crystallinity or length of P3HT, the addition of about ~5 wt% P3HT will lead to a change in the structure of the template.

Soft Matter Page 40 of 51

Moreover, order is also lost in all P3HT samples when there is an overloading of the system. At the extremes we measured for temperature, weight percentages, and molecular weight (10-15 wt% 77 kDa RRe-P3HT processed at 250 °C) the structure is affected drastically, leading to a collapse of structure and decreased order.

Composite blend samples can also be flow-aligned at the higher temperatures, leading to an ordered and oriented structure. By using a rectangular shim and creating a constrained flow route during the heat pressing stage, the material is forced to flow in an intended direction. During this process the domains orient in the direction of flow as the predicted morphology is shown in **Figure 13c**. This is observed in 2D SAXS images (**Figure 12**), with a clear increase in orientation between radially pressed and intentionally aligned samples. All flow-aligned samples were indexed to be hexagonally packed cylinders (**Figure S14**), but with the changed processing method, we believe the mixed phases align at different rates. We anticipate the hexagonally packed cylinder domains are easier to align than the lamellar domains, leading to disproportionate alignment during flow (**Figure 11**). The region of intermediate P3HT loadings that were identified as mixed and lamellar-rich phases in unaligned samples showed significantly less alignment which we anticipate could be due to differences in alignment of cylindrical vs lamellar domains.

Within the flow-aligned series we also see variation in the extent of alignment as the weight percent of RRe-P3HT increases. For pure PS-PI-PS, which forms consistent hexagonally packed cylinders, the material aligns well and there are no signs of orientation at orthogonal directions (**Figure 11**). When more conjugated polymer is added and the phase shifts towards mixed phases, domains begin to orient in inconsistent directions. At P3HT loadings of 2.5 - 7.5 wt% there are evident features in the flow direction, which is indicative of poor macroscopic orientation. This may be a result of the ease of alignment varying for regions within mixed phase samples, as the

Page 41 of 51 Soft Matter

material flow aligned the cylinders while the leaving the lamellar domains less aligned. At higher loadings, 12.5 and 15 wt% of RRe-P3HT, the matrix structure is more disordered but identified as primarily consisting of hexagonally packed cylinders. In this region, the system again shows improved alignment and orientation. There appears to be a relationship between the ability to align a flowed polymer blend and its phase make-up, with more consistent blends producing higher orientation.

5. Conclusions

In this work we utilized SANS, USAXS and SAXS to characterize complex blends of conjugated polymers and elastomeric copolymers while understanding the effect of temperature, composition, and processing. We determined that temperature is a vital consideration in processing blends of conjugated polymers and thermoplastic elastomers, with increased temperature allowing for system wide changes. Temperatures well above the glass transition temperature of the matrix and above the melting temperature of the conjugated polymer allow for increased consistency of the structures as well as increased incorporation of additives into the established structure. The PS-PI-PS elastomer forms a hexagonal cylinder template structure, and when P3HT is added into the blend, it integrates into the polyisoprene bulk surrounding polystyrene cylinders. Increased addition of P3HT additives modifies the phase of the matrix elastomer system with a critical concentration around 5 wt% that marks the maximum amount of P3HT that can be added while preserving high order in blends. Continuing to increase P3HT loading (wt%), a second threshold is reached around 10 wt% where the system increases in disorder, likely due to overloading and macro phase separation. The molecular weight of the conjugated polymer has a slight effect on how the additive is incorporated at higher processing temperatures, but changes are small with

Soft Matter Page 42 of 51

only significant changes in the 5 wt% critical concentration. These systems can also be macroscopically aligned through the use of directed flow during processing, and the extent of orientation of the phases in the system are dependent on the type and concentration of additives in the composite sample. In coexisting phases of cylinders and lamella seen around the 5 wt% P3HT critical concentration, the bulk material orients less cohesively and cylindrical portions flow to a greater extent than lamellar structures. This work aids in understanding the fundamental structural morphology of these complex copolymer blends, but additional work will be necessary to understand how these structural modifications can be utilized for property optimization. In depth use of imaging techniques such as transmission electron microscopy^{25,32,54} and atomic force microscopy^{78,79} have been used on PS-PI-PS systems previously. However, these are limited to the analysis of superficial structural organization and results can differ substantially from the bulk organization that SAXS is able to probe. Finally, the combination of molecular dynamics and experiments could further enable probing the molecular organization and dynamics in mixed blends as used in Guilbert et al's work on P3HT with PCBM⁸⁰. However, such calculations can be exceedingly costly for the large-scale phase segregation (10's of nm) that is observed in blockcopolymer systems showcased in this work. Coarse-grained simulations with appropriately parameterized force fields may be more feasible, relevant and insightful in future work.

Conflicts of Interest

There are no conflicts of interest to declare.

Data Availability

The data supporting this article have been included as part of the Supplementary Information

Page 43 of 51 Soft Matter

Acknowledgements

Primary support for this work was provided by the Department of Energy Office of Basic Energy Sciences under award number DE-SC0019911, which directly supported the research participation of all authors and the procurement of materials. The authors acknowledge the use of facilities and instrumentation supported by the U.S. National Science Foundation through the Major Research Instrumentation (MRI) program (DMR-2116265) and the UW Molecular Engineering Materials Center (MEM-C), a Materials Research Science and Engineering Center (DMR-2308979). This research was heavily informed by data run at the Advanced Photon Source; a U.S. Department of Energy (DOE) Office of Science User Facility operated for the DOE Office of Science by Argonne National Laboratory under contract no. DE-AC02-06CH11357. We thank the beamline scientists Jan Ilavsky and Ivan Kuzmenko at 9-ID for their contributions during preparation and remote collection of preliminary data for this experiment. This research uses the resources of the Australian Nuclear Science and Technology Organisation supported through ANSTO beamline award 15580 on Quokka Small Angle Neutron Scattering Instrument. This work also benefited from the use of the SasView application, originally developed under NSF award DMR-0520547. SasView contains a code developed with funding from the European Union's Horizon 2020 research and innovation program under the SINE2020 project, grant agreement no. 654000.

Soft Matter Page 44 of 51

Supporting Information:

Additional material characterization, data analysis, and supporting experiments discussed in pdf file, as well as additional file containing raw data of all samples discussed.

References

- (1) Sekine, T.; Sugano, R.; Tashiro, T.; Sato, J.; Takeda, Y.; Matsui, H.; Kumaki, D.; Dos Santos, F. D.; Miyabo, A.; Tokito, S. Fully Printed Wearable Vital Sensor for Human Pulse Rate Monitoring Using Ferroelectric Polymer. *Scientific Reports 2018 8:1* **2018**, *8* (1), 1–10. https://doi.org/10.1038/s41598-018-22746-3.
- (2) Ha, M.; Lim, S.; Ko, H. Wearable and Flexible Sensors for User-Interactive Health-Monitoring Devices. *J Mater Chem B* **2018**, *6* (24), 4043–4064. https://doi.org/10.1039/C8TB01063C.
- (3) Amjadi, M.; Kyung, K.-U.; Park, I.; Sitti, M.; Amjadi, M.; Sitti, M.; Kyung, K.; Park, I. Stretchable, Skin-Mountable, and Wearable Strain Sensors and Their Potential Applications: A Review. *Adv Funct Mater* **2016**, *26* (11), 1678–1698. https://doi.org/10.1002/ADFM.201504755.
- (4) Wang, S.; Oh, J. Y.; Xu, J.; Tran, H.; Bao, Z. Skin-Inspired Electronics: An Emerging Paradigm. Acc Chem Res 2018, 51 (5), 1033–1045. https://doi.org/10.1021/ACS.ACCOUNTS.8B00015/ASSET/IMAGES/LARGE/AR-2018-000159_0010.JPEG.
- (5) Khalili, N.; Naguib, H. E.; Kwon, R. H. A Constriction Resistance Model of Conjugated Polymer Based Piezoresistive Sensors for Electronic Skin Applications. *Soft Matter* **2016**, *12* (18), 4180–4189. https://doi.org/10.1039/C6SM00204H.
- (6) Benight, S. J.; Wang, C.; Tok, J. B. H.; Bao, Z. Stretchable and Self-Healing Polymers and Devices for Electronic Skin. *Prog Polym Sci* **2013**, *38* (12), 1961–1977. https://doi.org/10.1016/J.PROGPOLYMSCI.2013.08.001.
- (7) Jeon, K. H.; Park, J. W. Light-Emitting Polymer Blended with Elastomers for Stretchable Polymer Light-Emitting Diodes. *Macromolecules* 2022, 55 (18), 8311–8320. https://doi.org/10.1021/ACS.MACROMOL.2C01095/ASSET/IMAGES/LARGE/MA2C01095_0004.JP EG.
- (8) White, M. S.; Kaltenbrunner, M.; Głowacki, E. D.; Gutnichenko, K.; Kettlgruber, G.; Graz, I.; Aazou, S.; Ulbricht, C.; Egbe, D. A. M.; Miron, M. C.; Major, Z.; Scharber, M. C.; Sekitani, T.; Someya, T.; Bauer, S.; Sariciftci, N. S. Ultrathin, Highly Flexible and Stretchable PLEDs. *Nature Photonics 2013* 7:10 2013, 7 (10), 811–816. https://doi.org/10.1038/nphoton.2013.188.
- (9) Koo, J. H.; Kim, D. C.; Shim, H. J.; Kim, T. H.; Kim, D. H. Flexible and Stretchable Smart Display: Materials, Fabrication, Device Design, and System Integration. *Adv Funct Mater* **2018**, *28* (35), 1801834. https://doi.org/10.1002/ADFM.201801834.
- (10) Tait, J. G.; Worfolk, B. J.; Maloney, S. A.; Hauger, T. C.; Elias, A. L.; Buriak, J. M.; Harris, K. D. Spray Coated High-Conductivity PEDOT:PSS Transparent Electrodes for Stretchable and Mechanically-

Page 45 of 51 Soft Matter

- Robust Organic Solar Cells. *Solar Energy Materials and Solar Cells* **2013**, *110*, 98–106. https://doi.org/10.1016/J.SOLMAT.2012.09.005.
- (11) Lee, C. P.; Lai, K. Y.; Lin, C. A.; Li, C. T.; Ho, K. C.; Wu, C. I.; Lau, S. P.; He, J. H. A Paper-Based Electrode Using a Graphene Dot/PEDOT:PSS Composite for Flexible Solar Cells. *Nano Energy* **2017**, *36*, 260–267. https://doi.org/10.1016/J.NANOEN.2017.04.044.
- (12) Yang, Z.; Deng, J.; Sun, X.; Li, H.; Peng, H.; Yang, Z.; Deng, J.; Sun, X.; Li, H.; Peng, H. Stretchable, Wearable Dye-Sensitized Solar Cells. *Advanced Materials* **2014**, *26* (17), 2643–2647. https://doi.org/10.1002/ADMA.201400152.
- (13) Kang, D. Y.; Kim, Y. S.; Ornelas, G.; Sinha, M.; Naidu, K.; Coleman, T. P. Scalable Microfabrication Procedures for Adhesive-Integrated Flexible and Stretchable Electronic Sensors. *Sensors* (*Switzerland*) **2015**, *15* (9), 23459–23476. https://doi.org/10.3390/s150923459.
- (14) Wang, L.; Zhang, Y.; Pan, J.; Peng, H. Stretchable Lithium-Air Batteries for Wearable Electronics. *J Mater Chem A Mater* **2016**, *4* (35), 13419–13424. https://doi.org/10.1039/C6TA05800K.
- (15) Song, E.; Kang, B.; Ho Choi, H.; Hun Sin, D.; Lee, H.; Hyoung Lee, W.; Cho, K.; Song, E.; Kang, B.; Choi, H. H.; Sin, D. H.; Lee, H.; Cho, K.; Lee, W. H. Stretchable and Transparent Organic Semiconducting Thin Film with Conjugated Polymer Nanowires Embedded in an Elastomeric Matrix. *Adv Electron Mater* **2016**, *2* (1), 1500250. https://doi.org/10.1002/AELM.201500250.
- (16) Zhu, Y.; Li, N.; Lv, T.; Yao, Y.; Peng, H.; Shi, J.; Cao, S.; Chen, T. Ag-Doped PEDOT:PSS/CNT Composites for Thin-Film All-Solid-State Supercapacitors with a Stretchability of 480%. *J Mater Chem A Mater* **2018**, *6* (3), 941–947. https://doi.org/10.1039/C7TA09154K.
- (17) Song, R.; Schrickx, H.; Balar, N.; Siddika, S.; Sheikh, N.; O'connor, B. T. Unveiling the Stress–Strain Behavior of Conjugated Polymer Thin Films for Stretchable Device Applications. **2020**. https://doi.org/10.1021/acs.macromol.9b02573.
- (18) Liu, D.; Ding, Z.; Wu, Y.; Liu, S. F.; Han, Y.; Zhao, K. In Situ Study of Molecular Aggregation in Conjugated Polymer/Elastomer Blends toward Stretchable Electronics. *Macromolecules* 2022, 55 (1), 297–308. https://doi.org/10.1021/ACS.MACROMOL.1C01537/ASSET/IMAGES/LARGE/MA1C01537_0009.JP EG.
- (19) Billiet, S.; Hillewaere, X. K. D.; Teixeira, R. F. A.; Du Prez, F. E. Chemistry of Crosslinking Processes for Self-Healing Polymers. *Macromol Rapid Commun* 2013, 34 (4), 290–309. https://doi.org/10.1002/MARC.201200689.
- (20) Burfield, D. R. Polymer Glass Transition Temperatures. *Burfield, D. R. Polym. Commun* **1984**, *61* (2), 2.
- (21) Rieger, J. The Glass Transition Temperature of Polystyrene. Results of a Round Robin Test. *Journal of Thermal Analysis* **1996**, *46* (3–4), 965–972. https://doi.org/10.1007/BF01983614/METRICS.
- (22) Inoue, T.; Moritani, M.; Hashimoto, T.; Kawai, H. Deformation Mechanism of Elastomeric Block Copolymers Having Spherical Domains of Hard Segments under Uniaxial Tensile Stress1. *Macromolecules* **1970**, *8* (111), 579.

Soft Matter Page 46 of 51

- (23) Eugene Helfand; Z. R. Wasserman. Block Copolymer Theory. 6. Cylindrical Domains. *American Chemical Society* **1980**, 994–998.
- (24) Widin, J. M.; Schmitt, A. K.; Schmitt, A. L.; Im, K.; Mahanthappa, M. K. Unexpected Consequences of Block Polydispersity on the Self-Assembly of ABA Triblock Copolymers. *J Am Chem Soc* **2012**, 134 (8), 3834–3844. https://doi.org/10.1021/JA210548E/SUPPL_FILE/JA210548E_SI_001.PDF.
- (25) Hadziioannou, G.; Skoulios, A. Molecular Weight Dependence of Lamellar Structure in Styrene/Isoprene Two-and Three-Block Copolymers. *Separation Methods in Biochemistry* **1970**, 131 (1), 533.
- (26) Sakurai, S.; Aida, S.; Okamoto, S.; Ono, T.; Imaizumi, K.; Nomura, S. Preferential Orientation of Lamellar Microdomains Induced by Uniaxial Stretching of Cross-Linked Polystyrene-Block-Polybutadiene-Block-Polystyrene Triblock Copolymer. **2001**. https://doi.org/10.1021/ma002123.
- (27) Vukovic, I.; Brinke, G. Ten; Loos, K. Block Copolymer Template-Directed Synthesis of Well-Ordered Metallic Nanostructures. *Polymer (Guildf)* **2013**, *54* (11), 2591–2605. https://doi.org/10.1016/J.POLYMER.2013.03.013.
- (28) Laurer, J. H.; Hajduk, D. A.; Fung, J. C.; Sedat, J. W.; Smith, S. D.; Gruner, S. M.; Agard, D. A.; Spontak, R. J. Microstructural Analysis of a Cubic Bicontinuous Morphology in a Neat SIS Triblock Copolymer. *Macromolecules* **1997**, *30* (13), 3938–3941. https://doi.org/10.1021/MA970449L/ASSET/IMAGES/LARGE/MA970449LF00004.JPEG.
- (29) Pedemonte, E.; Turturro, A.; Bianchi, U.; Devetta, P. The Cubic Structure of a SIS Three Block Copolymer. *Polymer (Guildf)* **1973**, *14* (4), 145–150. https://doi.org/10.1016/0032-3861(73)90107-9.
- (30) Matsen, M. W.; Bates, F. S. Unifying Weak- and Strong-Segregation Block Copolymer Theories. *Macromolecules* **1996**, *29* (4), 1091–1098. https://doi.org/10.1021/MA951138I/ASSET/IMAGES/LARGE/MA951138IF00005.JPEG.
- (31) Sakurai, S.; Umeda, H.; Taie, K.; Nomura, S. Kinetics of Morphological Transition in Polystyrene-Block-Polybutadiene-Block-Polystyrene Triblock Copolymer Melt. *J. Chem. Phys* **1996**, *105*, 8902–8908. https://doi.org/10.1063/1.472619.
- Qiao, L.; Leibig, C.; Hahn, S. F.; Winey, K. I. Isolating the Effects of Morphology and Chain Architecture on the Mechanical Properties of Triblock Copolymers. *Ind Eng Chem Res* 2006, 45 (16), 5598–5602. https://doi.org/10.1021/IE0511940/ASSET/IMAGES/LARGE/IE0511940F00003.JPEG.
- (33) Inoue T; Soen T; Hashimoto T; Kawai H. Thermodynamic Interpretation of Domain Structure in Solvent-Cast Films of A–B Type Block Copolymers of Styrene and Isoprene. *Journal of Polymer Science Part A-2: Polymer Physics* **1969**, *7* (8), 1283–1301. https://doi.org/10.1002/POL.1969.160070801.
- (34) Séguéla, R.; Prud'homme, J. Deformation Mechanism of Thermoplastic Two-Phase Elastomers of Lamellar Morphology Having a High Volume Fraction of Rubbery Microphase. *Macromolecules* **1981**, *14*, 197–202.

Page 47 of 51 Soft Matter

- (35) Bokobza, L. Multiwall Carbon Nanotube Elastomeric Composites: A Review. *Polymer (Guildf)* **2007**, *48* (17), 4907–4920. https://doi.org/10.1016/J.POLYMER.2007.06.046.
- (36) Perez, L. D.; Zuluaga, M. A.; Kyu, T.; Mark, J. E.; Lopez, B. L. Preparation, Characterization, and Physical Properties of Multiwall Carbon Nanotube/Elastomer Composites. *Polym Eng Sci* **2009**, *49* (5), 866–874. https://doi.org/10.1002/PEN.21247.
- (37) Xu, J.; Wang, S.; Wang, G. J. N.; Zhu, C.; Luo, S.; Jin, L.; Gu, X.; Chen, S.; Feig, V. R.; To, J. W. F.; Rondeau-Gagné, S.; Park, J.; Schroeder, B. C.; Lu, C.; Oh, J. Y.; Wang, Y.; Kim, Y. H.; Yan, H.; Sinclair, R.; Zhou, D.; Xue, G.; Murmann, B.; Linder, C.; Cai, W.; Tok, J. B. H.; Chung, J. W.; Bao, Z. Highly Stretchable Polymer Semiconductor Films through the Nanoconfinement Effect. *Science* (1979) 2017, 355 (6320). https://doi.org/10.1126/SCIENCE.AAH4496/SUPPL_FILE/XU.SM.PDF.
- (38) Choi, D.; Kim, H.; Persson, N.; Chu, P. H.; Chang, M.; Kang, J. H.; Graham, S.; Reichmanis, E. Elastomer-Polymer Semiconductor Blends for High-Performance Stretchable Charge Transport Networks. Chemistry of Materials 2016, 28 (4), 1196–1204. https://doi.org/10.1021/ACS.CHEMMATER.5B04804/ASSET/IMAGES/CM-2015-04804F M002.GIF.
- (39) Carpi, F.; Gallone, G.; Galantini, F.; De Rossi Carpi, D. F.; De Rossi, D. Enhancement of the Electromechanical Transduction Properties of a Silicone Elastomer by Blending with a Conjugated Polymer. https://doi.org/10.1117/12.776641 2008, 6927 (10), 47–57. https://doi.org/10.1117/12.776641.
- (40) Qiu, Z.; Hammer, B. A. G.; Müllen, K. Conjugated Polymers Problems and Promises. *Progress in Polymer Science*. Elsevier Ltd January 1, 2020. https://doi.org/10.1016/j.progpolymsci.2019.101179.
- (41) Savagatrup, S.; Printz, A. D.; Rodriquez, D.; Lipomi, D. J. Best of Both Worlds: Conjugated Polymers Exhibiting Good Photovoltaic Behavior and High Tensile Elasticity. *Macromolecules* 2014, 47 (6), 1981–1992. https://doi.org/10.1021/MA500286D/ASSET/IMAGES/LARGE/MA-2014-00286D_0008.JPEG.
- (42) Shim, H. J.; Sunwoo, S. H.; Kim, Y.; Koo, J. H.; Kim, D. H. Functionalized Elastomers for Intrinsically Soft and Biointegrated Electronics. *Adv Healthc Mater* **2021**, *10* (17), 2002105. https://doi.org/10.1002/ADHM.202002105.
- (43) Shin, M.; Hyuk Song, J.; Lim, G.-H.; Lim, B.; Park, J.-J.; Jeong, U.; Shin, M.; Song, J. H.; Jeong, U.; Lim, G.; Lim, B.; Park, J. Highly Stretchable Polymer Transistors Consisting Entirely of Stretchable Device Components. *Advanced Materials* **2014**, *26* (22), 3706–3711. https://doi.org/10.1002/ADMA.201400009.
- (44) Wang, M.; Baek, P.; Akbarinejad, A.; Barker, D.; Travas-Sejdic, J. Conjugated Polymers and Composites for Stretchable Organic Electronics. *J Mater Chem C Mater* **2019**, *7* (19), 5534–5552. https://doi.org/10.1039/C9TC00709A.
- (45) Güldal, N. S.; Kassar, T.; Berlinghof, M.; Ameri, T.; Osvet, A.; Pacios, R.; Li Destri, G.; Unruh, T.; Brabec, C. J. Real-Time Evaluation of Thin Film Drying Kinetics Using an Advanced, Multi-Probe

Soft Matter Page 48 of 51

- Optical Setup. *J Mater Chem C Mater* **2016**, *4* (11), 2178–2186. https://doi.org/10.1039/C5TC03448E.
- (46) Cummings, J.; Lowengrub, J. S.; Sumpter, B. G.; Wise, S. M.; Kumar, R. Modeling Solvent Evaporation during Thin Film Formation in Phase Separating Polymer Mixtures. *Soft Matter* **2018**, 14 (10), 1833–1846. https://doi.org/10.1039/C7SM02560B.
- (47) Shi, W.; Li, W.; Delaney, K. T.; Fredrickson, G. H.; Kramer, E. J.; Ntaras, C.; Avgeropoulos, A.; Lynd, N. A. Morphology Re-Entry in Asymmetric PS-PI-PS' Triblock Copolymer and PS Homopolymer Blends. *J Polym Sci B Polym Phys* **2016**, *54* (2), 169–179. https://doi.org/10.1002/POLB.23811.
- (48) Albalak, R. J.; Thomas, E. L.; Capel, M. S. Thermal Annealing of Roll-Cast Triblock Copolymer Films. *Polymer (Guildf)* **1997**, *38* (15), 3819–3825. https://doi.org/10.1016/S0032-3861(96)00938-X.
- (49) Hadziioannou, G.; Skoulios, A. Melting of Styrene/Isoprene Block Copolymers as a Function of Temperature and Time. *Physics of Glassy Polymers* **1975**, *148* (1), 3483.
- (50) Wolf, C. M.; Guio, L.; Scheiwiller, S. C.; O'Hara, R. P.; Luscombe, C. K.; Pozzo, L. D. Blend Morphology in Polythiophene–Polystyrene Composites from Neutron and X-Ray Scattering. *Macromolecules* **2021**. https://doi.org/10.1021/acs.macromol.0c02512.
- (51) Lim, H.; Chao, C.-Y.; Su, W.-F. Modulating Crystallinity of Poly(3-Hexylthiophene) via Microphase Separation of Poly(3-Hexylthiophene)–Polyisoprene Block Copolymers. **2015**. https://doi.org/10.1021/ma502417w.
- (52) Olsen, B. D.; Shah, M.; Ganesan, V.; Segalman, R. A. Universalization of the Phase Diagram for a Model Rod-Coil Diblock Copolymer. *Macromolecules* 2008, 41 (18), 6809–6817. https://doi.org/10.1021/MA800978C/ASSET/IMAGES/LARGE/MA-2008-00978C_0010.JPEG.
- (53) Lin, S. H.; Wu, S. J.; Ho, C. C.; Su, W. F. Rational Design of Versatile Self-Assembly Morphology of Rod-Coil Block Copolymer. *Macromolecules* 2013, 46 (7), 2725–2732. https://doi.org/10.1021/MA302220B/SUPPL_FILE/MA302220B_SI_001.PDF.
- (54) Georgopanos, P.; Rangou, S.; Gil Haenelt, T.; Abetz, C.; Meyer, A.; Filiz, V.; Handge, U. A.; Abetz, V. Analysis of Glass Transition and Relaxation Processes of Low Molecular Weight Polystyrene-b-Polyisoprene Diblock Copolymers. *Colloid Polym Sci* 2014, 292 (8), 1877–1891. https://doi.org/10.1007/S00396-014-3284-Y/FIGURES/7.
- (55) Heeley, E. L.; Gough, T.; Hughes, D. J.; Bras, W.; Rieger, J.; Ryan, A. J. Effect of Processing Parameters on the Morphology Development during Extrusion of Polyethylene Tape: An in-Line Small-Angle X-Ray Scattering (SAXS) Study. **2013**. https://doi.org/10.1016/j.polymer.2013.10.004.
- (56) Roesing, M.; Howell, J.; Boucher, D. Solubility Characteristics of Poly(3-Hexylthiophene). *J. Polym. Sci., Part B: Polym. Phys* **2017**, *55*, 1075–1087. https://doi.org/10.1002/polb.24364.
- (57) Teresa García, M.; Gracia, I.; Duque, G.; de Lucas, A.; Francisco Rodríguez, J. Study of the Solubility and Stability of Polystyrene Wastes in a Dissolution Recycling Process. 2009. https://doi.org/10.1016/j.wasman.2009.01.001.

Page 49 of 51 Soft Matter

- (58) Yamazaki, H.; Nagasawa, T.; Choi, W.; Endo, T. Transformation of Vulcanized Natural Rubber into Lower Molecular Weight Polymers and Their Application to Grafted Copolymer Synthesis with Some Vinyl Monomers. *J Appl Polym Sci* **2006**, *101* (6), 4003–4010. https://doi.org/10.1002/APP.22964.
- (59) Doucet, M.; King, S.; Butler, P.; Kienzle, P.; Parker, P.; Krzywon, J.; Jackson, A.; Richter, T.; Gonzales, M.; Nielsen, T.; Ferraz, L. R. SasView. 2022.
- (60) Doucet, M.; King, S.; Butler, P.; Kienzle, P.; Parker, P.; Krzywon, J.; Jackson, A.; Richter, T.; Gonzales, M.; Nielsen, T.; Ferraz, L. R. Sasmodels. 2020.
- (61) Kienzle, P. A. (Unviversity of M. C. P.; Krycka, J.; Patel, N.; Sahin, I. Bumps. 2011.
- (62) Wood, K.; Mata, J. P.; Garvey, C. J.; Wu, C. M.; Hamilton, W. A.; Abbeywick, P.; Bartlett, D.; Bartsch, F.; Baxter, P.; Booth, N.; Brown, W.; Christoforidis, J.; Clowes, D.; d'Adam, T.; Darmann, F.; Deura, M.; Harrison, S.; Hauser, N.; Horton, G.; Federici, D.; Franceschini, F.; Hanson, P.; Imamovic, E.; Imperia, P.; Jones, M.; Kennedy, S.; Kim, S.; Lam, T.; Lee, W. T.; Lesha, M.; Mannicke, D.; Noakes, T.; Olsen, S. R.; Osborn, J. C.; Penny, D.; Perry, M.; Pullen, S. A.; Robinson, R. A.; Schulz, J. C.; Xiong, N.; Gilbert, E. P. QUOKKA, the Pinhole Small-Angle Neutron Scattering Instrument at the OPAL Research Reactor, Australia: Design, Performance, Operation and Scientific Highlights. urn:issn:1600-5767 2018, 51 (2), 294–314. https://doi.org/10.1107/S1600576718002534.
- (63) Kline, S. R.; IUCr. Reduction and Analysis of SANS and USANS Data Using IGOR Pro. *urn:issn:0021-8898* **2006**, *39* (6), 895–900. https://doi.org/10.1107/S0021889806035059.
- (64) broad_peak SasView 5.0.5 documentation. https://www.sasview.org/docs/user/models/broad_peak.html (accessed 2022-09-01).
- (65) Hammouda, B.; IUCr. A New Guinier–Porod Model. *urn:issn:0021-8898* **2010**, *43* (4), 716–719. https://doi.org/10.1107/S0021889810015773.
- (66) Pedersen, J. S.; Schurtenberger, P. Scattering Functions of Semiflexible Polymers with and without Excluded Volume Effects. *Macromolecules* **1996**, *29* (23), 7602–7612. https://doi.org/10.1021/MA9607630/ASSET/IMAGES/MEDIUM/MA9607630E00030.GIF.
- (67) Xi, Y.; Wolf, C. M.; Pozzo, L. D. Self-Assembly of Donor–Acceptor Conjugated Polymers Induced by Miscible 'Poor' Solvents. Soft Matter 2019, 15 (8), 1799–1812. https://doi.org/10.1039/C8SM02517G.
- (68) Harris, C. R.; Jarrod Millman, K.; van der Walt, S. J.; Gommers, R.; Virtanen, P.; Cournapeau, D.; Wieser, E.; Taylor, J.; Berg, S.; Smith, N. J.; Kern, R.; Picus, M.; Hoyer, S.; van Kerkwijk, M. H.; Brett, M.; Haldane, A.; Fernández del Río, J.; Wiebe, M.; Peterson, P.; Gérard-Marchant, P.; Sheppard, K.; Reddy, T.; Weckesser, W.; Abbasi, H.; Gohlke, C.; Oliphant, T. E. Array Programming with NumPy. *Nature* **2020**, *585*, 357. https://doi.org/10.1038/s41586-020-2649-2.
- (69) Mckinney, W. Data Structures for Statistical Computing in Python. 2010.
- (70) Hunter, J. D. Matplotlib: A 2D Graphics Environment. *Comput Sci Eng* **2007**, *9* (3), 90–95. https://doi.org/10.1109/MCSE.2007.55.

Soft Matter Page 50 of 51

- (71) McNeill, I. C.; Gupta, S. N. Degradation of Blends Part XI. Blends of Polystyrene with Polyisoprene. *Polym Degrad Stab* **1980**.
- (72) Mcneill, I. C. Thermal Degradation of Polystyrene in Different Environments. *Die Angewandte Makromolekulare Chemie* **1997**, *247* (4432), 179–195. https://doi.org/10.1002/apmc.1997.052470112.
- (73) Rodrigues, A.; Castro, M. C. R.; Farinha, A. S. F.; Oliveira, M.; Tomé, J. P. C.; Machado, A. V.; Raposo, M. M. M.; Hilliou, L.; Bernardo, G. Thermal Stability of P3HT and P3HT:PCBM Blends in the Molten State. *Polym Test* **2013**, *32* (7), 1192–1201. https://doi.org/10.1016/J.POLYMERTESTING.2013.07.008.
- (74) Balko, J.; Lohwasser, R. H.; Sommer, M.; Thelakkat, M.; Thurn-Albrecht, T. Determination of the Crystallinity of Semicrystalline Poly(3-Hexylthiophene) by Means of Wide-Angle X-Ray Scattering. **2023**, *21*, 38. https://doi.org/10.1021/ma401946w.
- (75) Qiu, L.; Lee, W. H.; Wang, X.; Kim, J. S.; Lim, J. A.; Kwak, D.; Lee, S.; Cho, K. Organic Thin-Film Transistors Based on Polythiophene Nanowires Embedded in Insulating Polymer. *Advanced Materials* **2009**, *21* (13), 1349–1353. https://doi.org/10.1002/adma.200802880.
- (76) Olsen, B. D.; Shah, M.; Ganesan, V.; Segalman, R. A. Universalization of the Phase Diagram for a Model Rod-Coil Diblock Copolymer. *Macromolecules* 2008, 41 (18), 6809–6817. https://doi.org/10.1021/MA800978C/ASSET/IMAGES/LARGE/MA-2008-00978C_0010.JPEG.
- (77) Emerson, J. A.; Toolan, D. T. W.; Howse, J. R.; Furst, E. M.; Epps, T. H. Determination of Solvent–Polymer and Polymer–Polymer Flory–Huggins Interaction Parameters for Poly(3-Hexylthiophene) via Solvent Vapor Swelling. *Macromolecules* **2013**, *46* (16), 6533–6540. https://doi.org/10.1021/MA400597J.
- (78) Phillips, J. P.; Deng, X.; Stephen, R. R.; Fortenberry, E. L.; Todd, M. L.; McClusky, D. M.; Stevenson, S.; Misra, R.; Morgan, S.; Long, T. E. Nano- and Bulk-Tack Adhesive Properties of Stimuli-Responsive, Fullerene–Polymer Blends, Containing Polystyrene-Block-Polybutadiene-Block-Polystyrene and Polystyrene-Block-Polyisoprene-Block-Polystyrene Rubber-Based Adhesives. *Polymer (Guildf)* **2007**, *48* (23), 6773–6781. https://doi.org/10.1016/J.POLYMER.2007.08.050.
- (79) Zhao, Y.; Ma, Y.; Xiong, Y.; Qin, T.; Zhu, Y.; Deng, H.; Qin, J.; Shi, X.; Zhang, G. Chemically Crosslinked Crystalline Thermoplastic Polyolefin Elastomer with Good Elasticity and Improved Thermo-Mechanical Properties. *Polymer (Guildf)* **2022**, *254*, 125075. https://doi.org/10.1016/J.POLYMER.2022.125075.
- (80) Guilbert, A. A. Y.; Zbiri, M.; Dunbar, A. D. F.; Nelson, J. Quantitative Analysis of the Molecular Dynamics of P3HT:PCBM Bulk Heterojunction. *Journal of Physical Chemistry B* **2017**, *121* (38), 9073–9080. https://doi.org/10.1021/ACS.JPCB.7B08312/ASSET/IMAGES/LARGE/JP-2017-08312U_0004.JPEG.

Page 51 of 51 Soft Matter

The data supporting this article has been included as part of the Supplementary Information. The data is separated by instrument and sample type and the readme that accompanies the data is reproduced below:

Data is organized by instrument (SANS, SAXS, USAXS, Thermal Analysis) and then experiment type. Each section has a csv/explainer document that specifies sample information (weight percent, temperature, pressing time, ect) for each sample.

For liquid SANS data, the data files are named with respect to the sample name, and a column in the sample information csv has specific file names if needed. For TGA/DCS data, the explainer document has sample to number information. For USAXS data, the data is tagged with meta data information including names of samples. This can be accessed in the Xenocs XSACT software or in the header when the file is read. For the SAXS information, data is labeled in the "comment" metadata with a 96 well plate location that can be correlated to a specific sample using the provided sample information CSVs.

All data is minimally processed. For SANS data the configurations are stitched, and the background is subtracted. For USAXS data, the data is scaled, and the empty beam subtracted and then trimmed to remove the main beam q values. For the SAXS data, the configurations are stitched, and the data is trimmed to accurate q ranges.